Engineering Structures 302 (2024) 117241

Contents lists available at ScienceDirect

Engineering Structures

journal homepage: www.elsevier.com/locate/engstruct

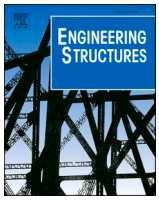

Load transfer of small-diameter GFRP and stainless steel doweled-joints in slabs-on-ground

Mohammed Fasil [a], Muhammad Kalimur Rahman [b,*], Mesfer M. Al-Zahrani [a,b], Antonio Nanni [c], Syed Khaja Najamuddin [a]

[a] Civil and Environmental Engineering Department, King Fahd University of Petroleum and Minerals (KFUPM), Dhahran, Saudi Arabia
[b] Interdisciplinary Research Center for Construction and Building Materials (IRC-CBM), KFUPM, Dhahran, Saudi Arabia
[c] Civil and Architectural Engineering Department, University of Miami, Coral Gables, FL, USA

ARTICLE INFO

Keywords:
Glass fiber-reinforced polymer (GFRP)
Dowels
Design wheel loads
Joint effectiveness (*E*)
Load transfer efficiency (*LTE*)
Relative deflection (Δ)
Stainless steel

ABSTRACT

Large diameter steel and glass fiber-reinforced polymer (GFRP) dowel bars are commonly used in rigid concrete pavements in highways for load transfer across joints to combat the concrete deterioration due to corrosion of steel dowels. Small-diameter GFRP dowel bars can be used at the expansion joints in slabs-on-ground, walkways, industrial floors and concrete-lined channels, which are not subjected to heavy traffic loads. This study investigated the performance and behavior of small-diameter GFRP dowels. GFRP dowels with three diameters (14 mm, 16 mm, and 38 mm) and stainless steel dowels (12 mm dia.) were embedded across a 25 mm-wide joint in a test slab with overall dimensions of 1500 × 750 × 200 mm^3. The variables of the study were the type of dowel material (GFRP and stainless steel), the diameter of GFRP dowels, the spacing of the dowels (200 mm and 250 mm c/c), and the type of loading (monotonic and cyclic). The slabs were loaded up to the failure of the joints under a concentrated load applied at the edge of the joint. The performance of the dowel-jointed slab specimens was investigated based on the cracking and ultimate loads, modes of failure, and load-displacement response. The ability of the small-diameter dowel bars to transfer displacements across the joint was quantified using the quantitative measures of joint effectiveness (*E*), load transfer efficiency (*LTE*), and relative deflections (Δ). Failure of the specimens with 14 mm and 16 mm diameter dowels occurred predominantly due to shear failure of the dowels before the cracking of concrete. However, for the specimens with large-diameter GFRP dowels and the stainless steel dowels, failure was associated with cracking of the concrete. A smaller spacing of the GFRP dowels and a longer embedment length gave a stiffer load-displacement response. Reducing the spacing from 250 mm to 200 mm resulted in a 4.1-fold reduction in relative deflection under the AASHTO H10 design wheel load (~35.6 kN). Increasing the dowel length had no significant effect on the load-carrying capacity of the dowel-jointed slabs. Cyclic load tests on the specimens revealed that the joint effectiveness (*E*) and the load transfer efficiency (*LTE*) of GFRP dowels were within the AASHTO and ACPA limits up to a concentrated load higher than the AASHTO HL93 dual tandem-axle wheel load (~55.6 kN).

1. Introduction

Transverse contraction joints are invariably provided in concrete pavements primarily to limit random cracking in concrete and to compensate for the thermal expansion of concrete [1]. The provision of joints at specific intervals increases the likelihood of uneven settlement in the slabs when subjected to moving wheel loads, particularly in the vicinity of the joints. Thus, it is crucial to provide an efficient means to effectively transfer loads across joints with minimal damage to concrete and to ensure a smooth ride. Dowels are the most common form of load transfer devices used in jointed slabs-on-ground and pavements to provide smooth transitions across joints, prevent deterioration and cracking, and control volumetric phenomena such as warping and curling caused by temperature and moisture gradients across the depth of the concrete slab-on-ground [2,3]. Durability and performance issues arising from corrosion of the commonly used steel dowels, including tensile cracks in the surrounding concrete caused by the accumulation of corrosion products and loss of dowel cross-section, lead to lower

* Corresponding author.
E-mail address: mkrahman@kfupm.edu.sa (M.K. Rahman).

https://doi.org/10.1016/j.engstruct.2023.117241
Received 20 October 2022; Received in revised form 22 November 2023; Accepted 25 November 2023

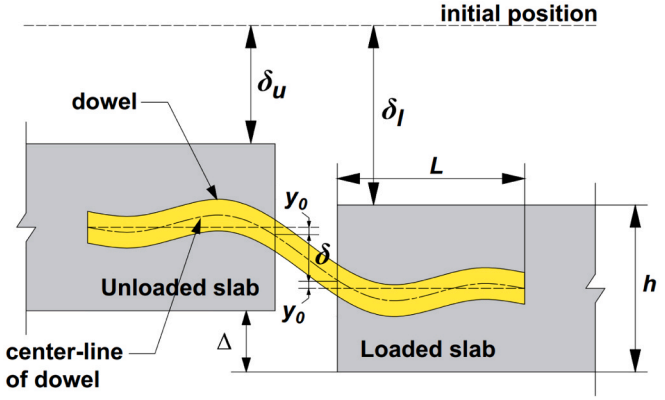

Fig. 1. Load transfer dowel-jointed slabs-on-ground: relative deflection.

efficiency in transferring loads and vertical displacements [4]. The accumulation of corrosion products would also lead to performance issues such as joint lockup leading to cracking of concrete [1,5]. Several US departments of transportation have reported that the use of epoxy-coated steel dowels does not always ensure a service life of more than 50 years, the duration for which highway rigid pavements are generally built to last, since epoxy coating is susceptible to damage during various phases of the pavement construction and service [6,7]. Newer alternatives to epoxy-coated steel bars including stainless steel, are significantly more expensive, resulting in higher project costs [8].

Recent advances in the field of polymer technologies have led to the emergence of glass fiber-reinforced polymer (GFRP) bars as a suitable alternative to conventional steel rebars, owing to their higher tensile strength, lower weight, non-corrosiveness, and ability to withstand deicing agents [8–11]. Furthermore, the smooth surface of GFRP dowel bars allows for a lesser bond at the GFRP-concrete interface, negating the need for a lubricant or bond-breaker mechanism, thereby reducing joint lockup significantly [12–14]. However, owing to the lower elastic modulus of GFRP dowels as compared to steel, studies have found that GFRP dowels should have a 20–30% larger diameter or closer spacing for comparable performance in terms of deflections, concrete bearing stresses, and load transfer efficiency in rigid pavements subjected to heavy truck loads [15,16].

The efficiency of joints in rigid pavements can be quantitatively assessed by several equations such as joint effectiveness (*E*), specified by the American Concrete Pavement Association (ACPA) code [17], load transfer efficiency (*LTE*), specified by the American Association of State Highway and Transportation Officials (AASHTO) code [18], and relative deflection (Δ) (Fig. 1). *E*, *LTE*, and Δ can be computed from experimental measurements using Eqs. 1, 2, and 3, respectively.

$$E = \frac{2\delta_u}{\delta_u + \delta_l} \times 100 \tag{1}$$

$$LTE = \frac{\delta_u}{\delta_l} \times 100 \tag{2}$$

$$\Delta = \delta_l - \delta_u \tag{3}$$

Here, δ_u is the unloaded slab deflection, and δ_l is the loaded slab deflection. For *E* and *LTE*, an efficiency of 100% indicates full transfer and 0% indicates no transfer at the joint between the loaded and unloaded slabs. The recommended joint effectiveness (*E*), according to ACPA is 75% [17], and the load transfer efficiency (*LTE*) recommended by AASHTO is 75% [18].

The design of dowels in rigid pavements is governed by the bearing stresses (σ_b) developed in concrete due to the load transferred by the dowel through the embedded part, as provided by ACI Committee 325 [19]. The bearing stress, σ_b should not exceed the allowable bearing stress of concrete (f_b), as given in Eq. 4.

$$\sigma_b = Ky_0 < \left[f_b = \frac{1}{3}(4 - d_b) f_c' \right] \tag{4}$$

where *K* is the modulus of dowel support and y_0 is the deflection of the dowel at the face of the concrete at the joint proposed by Friberg [20], assuming the dowel to be a beam and the concrete to be a Winkler foundation and based on the analysis of beam on elastic foundation provided by Timoshenko and Lessels [21]. The variable d_b is the diameter of the dowel bar (in m), f_b is the concrete permissible bearing stress and f_c' is the compressive strength of concrete. The value of y_0 and the relative stiffness of dowel in concrete (β) is given by:

$$y_0 = \frac{P_t(2 + \beta z)}{4\beta^3 E_d I} \tag{5}$$

$$\beta = \sqrt[4]{\frac{Kd_b}{4E_d I}} \tag{6}$$

where P_t is the load transferred by the critical dowel, *z* is the joint width, E_d is the modulus of elasticity, and *I* is the moment of inertia. The relative deflection across the joint (Δ) depends on the shear deformation of the dowel (δ) and y_0 given by Eq. 7 and Eq. 8.

$$\Delta = 2y_0 + \delta \tag{7}$$

$$\delta = \frac{\lambda P_t z}{AG} \tag{8}$$

where λ is the shear shape factor, *A* is the area of the dowel bar and *G* is the shear modulus (Fig. 1).

Studies have been conducted on the application of GFRP dowel bars as load transferring devices at joints in pavements [6,7,14,22,23]. Laboratory and field investigations on the performance of GFRP dowels conducted by Vijay et al. [22] found that GFRP bars performed satisfactorily when used as an alternative to steel dowels in jointed plain concrete pavements (JPCP). Load transfer efficiency (*LTE*) was found to exceed AASHTO code [18] and ACPA code [17] recommendations under static and fatigue load tests when GFRP dowels of larger diameters were used, which had flexural stiffness comparable with typical steel dowels. Benmokrane et al. [6] conducted laboratory and field tests to quantify the load transfer characteristics of 34.9 mm and 38.1 mm GFRP dowels and compared them with 28.6 mm steel dowels with a comparable flexural modulus. The flexural modulus (*EI*) of GFRP dowels with diameters 34.9 mm and 38.1 mm were calculated to be 3.66×10^9 Nmm^2 and 5.33×10^9 Nmm^2, respectively, while that of the 28.6 mm steel dowel was 6.57×10^9 Nmm^2, which are practically comparable. The specimens with 34.9 mm and 38.1 mm GFRP dowels exhibited ultimate capacities of 90.8% and 94.4%, respectively of the capacity of 28.6 mm steel dowels, while still maintaining similar failure modes and crack patterns. Upon cyclic loading for 1 million cycles at service loads, the GFRP dowels did not undergo any cracking,without compromising the efficiency of load transfer. In the field application, steel and GFRP dowel bars provided load transfer efficiencies (*LTE*) of approximately 87.9% and 88.6%, which is higher than the ACPA [17] recommended *LTE* value of 75%. Another research involving field investigations by Anderson et al. [7], also revealed that *LTE*s at joints, determined using falling weight reflectometers (FWD) with GFRP and epoxy-coated steel bars were very close to each other. Fatigue tests on GFRP dowels were conducted by Porter et al. [14] by applying 40 kN for 5 million cycles to study the effect of spacing of 38.1 mm GFRP dowel bars. The 40 kN wheel load corresponds to the ~9000 lb wheel load selected in AASHTO [18] to determine the joint performance parameters. The specimen with dowel spacing of 305 mm failed at 582,000 cycles, while the specimen with 152 mm spacing showed no failure at the end of the cycles. The study extrapolated that the failure of the latter would take place after 100 million cycles, which was much greater than the cycles expected

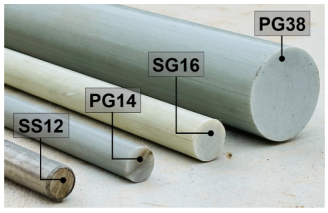

Fig. 2. Dowel bars used in the study.

Table 1
Materials properties.

Dowel bar name	PG14	SG16	PG38▲	SS12
Material type	GFRP			Stainless steel
Guaranteed tensile strength (MPa)*	870.9	799.3	517	683 (f_y)
Guaranteed transverse shear strength (MPa)*	152.6	155.8	150	0.6 f_y = 410 MPa
Young's modulus (GPa)	48.4	47	46	199
Diameter (mm)	13.7	16	38	12

Note: *Guaranteed strength for GFRP: Average strength - Thrice the standard deviation; ▲from the manufacturer's technical data sheet

during its service life. The stiffness of the subgrade material has a strong effect on the load-deflection response and load-transfer characteristics of a joint. The effect of subgrade material on the joint effectiveness (E) of GFRP dowels was studied by Eddie et al. [24]. According to the study, on a weak subgrade, the joint effectiveness ranged between 86% and 100%, while it varied between 90% and 97% on a stiff subgrade. Several studies have reported the use of compacted soil subgrade in laboratory experiments. However, with repeated tests on the same subgrade, the studies were unable to retain the same level of compaction for subsequent tests [25,26]. To overcome this issue, experimental research works by Øverli [27] and Manfredi et al. [28], extruded polystyrene foams were used to test the load-carrying capacity of a slab-on-ground specimen by subjecting it to concentrated loads.

Slabs-on-ground reinforced with GFRP bars have recently gained importance as it has been mandated for use in all grade-supported concrete structures, as a part of a major initiative in Saudi Arabia and worldwide towards the implementation of non-metallics in construction. This initiative led to the construction of a colossal 21.3 km-long flood mitigation channel in Jazan, Saudi Arabia with bed widths of up to 74 m and utilizing more than 10 million linear meters of GFRP bars from three different manufacturers from around the world [29–31]. All slabs in the channel are grade-supported with one layer of GFRP bars placed at 75 mm from the top of the 200 mm thick slab with a spacing of 200 mm center-to-center in both directions. These grade-supported slabs are distinct as they are not subjected to the same level and frequency of loads as rigid concrete in highway pavements. In the flood mitigation channel, stainless steel dowel bars were used at the expansion joints spaced at 30 m. The joints in the channel are expected to be subjected to infrequent loadings from maintenance trucks with low wheel loads only. For many slab-on-ground applications, GFRP dowel bars of smaller diameter could potentially be used at the joints, if the likelihood of heavy loads is low.

This paper presents the results of an experimental work conducted to investigate the effectiveness of small-diameter GFRP dowel bars (14 mm and 16 mm) in slabs-on-ground and its performance was compared to large diameter GFRP (38 mm) and stainless steel (12 mm) dowels. The joints with various dowel types between two plain concrete slabs were tested under concentrated loads, simulating wheel loads up to failure, and load-deflection responses at several key locations were captured in the slab specimens. Extruded polystyrene (XPS) foam was used as the subbase to simulate compacted soil subgrade. The study investigated the effect of parameters such as GFRP dowel diameter, material types, spacing, embedded length, dowel-end fixity, and type of loading. The performance of the dowel-jointed slab specimens was compared based on the load-displacement response, joint effectiveness (E), load transfer efficiency (LTE), relative deflection at joints (Δ), and dowel bar strains.

2. Experimental program

2.1. Materials

Two types of GFRP dowel bars, designated as PG and SG from two different manufacturers were selected for the study. The commercially available PG bars are ribbed, while the SG bars have a sand-coated surface. However, upon request, the manufacturers provided plain bars for the present study. Dowel bars are generally plain and smooth to maintain minimum friction between the dowel bars and concrete during thermal expansion [14]. Two diameters of GFRP dowel type PG (PG14 with 14 mm dia. and PG38 with 38 mm dia.) along with type SG (SG16

Table 2
Concrete properties.

Cement type and content	Aggregates (kg/m^3)			Admixtures (ml /m^3)		Mixing water (l/m^3)	28-day compressive strength (MPa)	
	20 mm	10 mm	Fine	PC 314*	D10§		Comp.	Tens.
Sulfate resisting cement (320 kg/m^3)	770	330	760	1300	2000	160	34.5	2.6

Note: *PC314: Fluidum PC314 high-efficiency liquid superplasticizer; §Arcrete D10: water reducer & set retarder

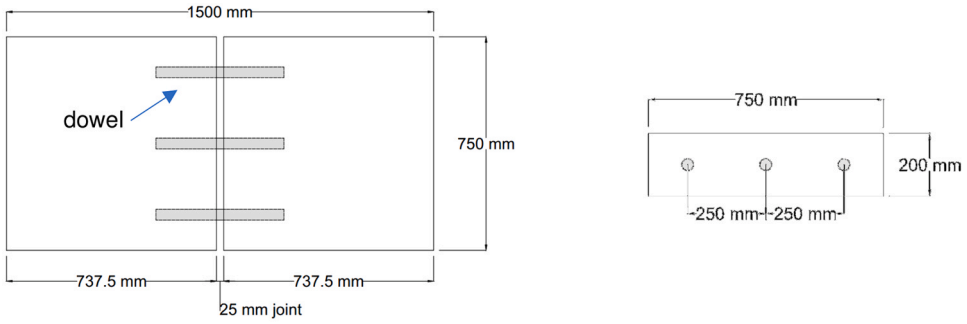

(a) Plan view (b) Section-view at joint face

Fig. 3. Schematic diagram of test prototype.

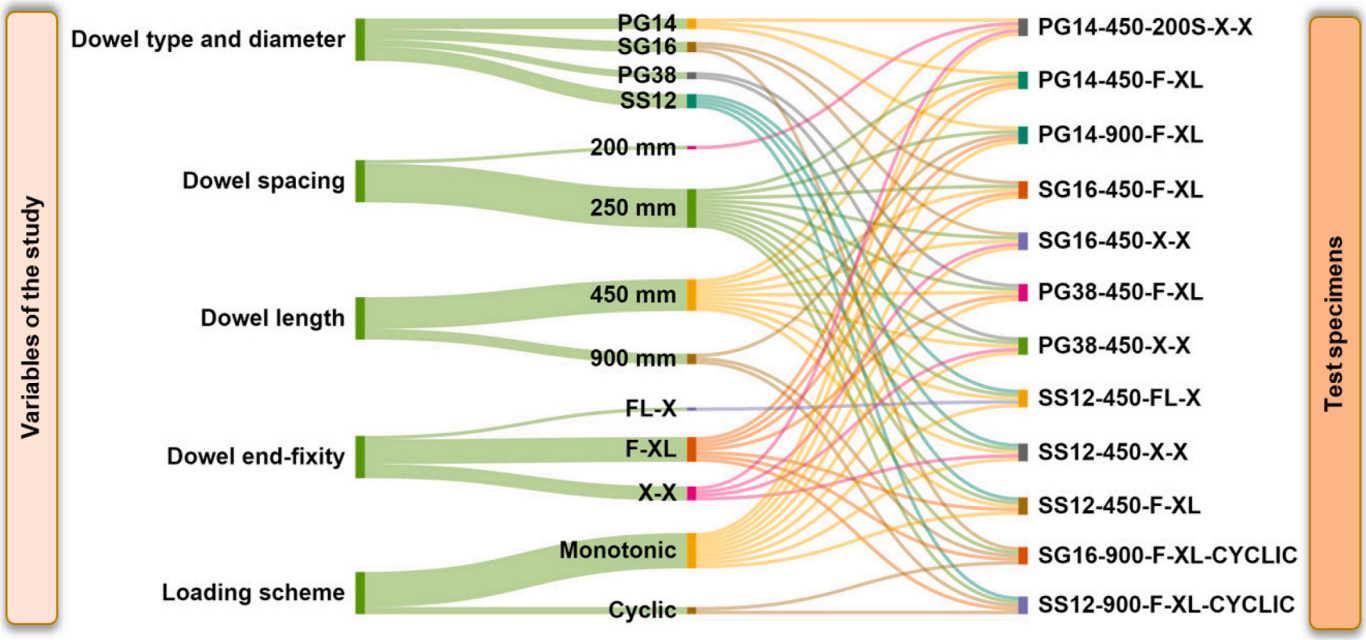

Fig. 4. Sankey diagram: test matrix.

Table 3
Test Matrix.

Sl. No.	Specimen ID	Dowel type	Dowel spacing (mm)	Dowel length (mm)	Dowel end-fixity	Loading scheme
1	PG14-450-200S-X-X	PG14	200	450	X-X	Monotonic
2	PG14-450-F-XL	PG14	250	450	F-XL	Monotonic
3	PG14-900-F-XL	PG14	250	900	F-XL	Monotonic
4	SG16-450-F-XL	SG16	250	450	F-XL	Monotonic
5	SG16-450-X-X	SG16	250	450	X-X	Monotonic
6	PG38-450-F-XL	PG38	250	450	F-XL	Monotonic
7	PG38-450-X-X	PG38	250	450	X-X	Monotonic
8	SS12-450-FL-X	SS12	250	450	FL-X	Monotonic
9	SS12-450-X-X	SS12	250	450	X-X	Monotonic
10	SS12-450-F-XL	SS12	250	450	F-XL	Monotonic
11	SG16-900-F-XL-CYCLIC	SG16	250	900	F-XL	Cyclic
12	SS12-900-F-XL-CYCLIC	SS12	250	900	F-XL	Cyclic

dowel with 16 mm dia.), were used in the experimental program (see Fig. 2). Stainless steel dowel bar of 12 mm dia., SS12, which was used in the flood mitigation channel in Jazan was also used in the study for comparative assessment with the GFRP dowels [29]. At the flood mitigation channel in Jazan, it was initially proposed to use small-diameter GFRP dowels at the expansion joints. However, due to the lack of performance data of small-diameter GFRP dowels, the small-diameter (12 mm) stainless steel dowels were adopted. The current research was primarily motivated by a lack of understanding regarding the behavior of small-diameter GFRP dowel bars in field applications. The properties of the dowel bars are shown in Table 1. The mix design and properties of the concrete used in the study for the construction of slabs are presented in Table 2. The target slump of concrete was 25 mm and the target 28-day compressive strength was 25 MPa. The compressive strength of concrete was tested according to ASTM C39M-21 [32], while the splitting tensile strength was tested as per ASTM C496–96 [33]. The dowel-jointed slab specimens were subjected to curing with burlaps and polythene sheets for seven days after casting. The specimens were tested approximately 6 months after the casting.

2.2. Test prototypes and parameters

The effectiveness of GFRP dowels was studied by fabricating and testing slab specimens with a doweled-joint in the laboratory. Twelve dowel-jointed slabs with various types of dowel bars, dowel end-fixities, dowel length and spacings, and loading types were constructed for load tests up to failure. The width of the joint was not a variable and was kept constant at 25 mm. According to ACI 325.12R-02 [34], a maximum width of 32 mm can be used for a doweled transverse expansion joint.

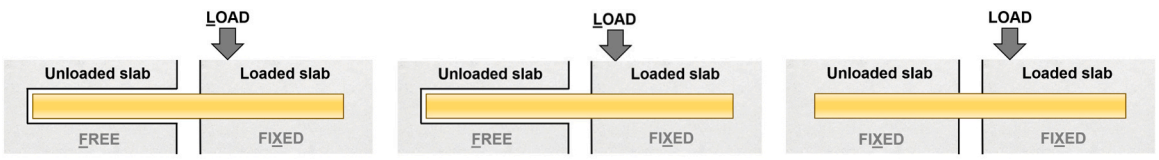

(a) F-XL (b) FL-X (c) X-X

Fig. 5. Dowel end-fixities.

(a) mold for PG38-450-F-XL: provision of joint, hooks for lifting, dowel supports for alignment

(b) molds prepared for casting

(c) specimens after de-molding

Fig. 6. Test prototypes.

Table 4
Design wheel loads.

AASHTO highway loading	Wheel load type	Design axle load (kN)	Design wheel load (kN)
H10	Single-axle (rear)	71.2	35.6
HS15	Single-axle (rear)	106.8	53.4
HL93	Dual tandem-axle (rear)	111.2	55.6
HL93	Single-axle (rear)	142.3	71.2

Researchers have been reported to use widths of 19 mm [6] and 21 mm [1]. Furthermore, in the flood mitigation channel in Jazan, Saudi Arabia, a joint width of 25 mm was used. The schematic diagram of the test specimen is shown in Fig. 3. The physical dimensions of the dowel-jointed slabs were determined based on numerical and experimental works in the literature [6,22,24,35]. The test prototype consisted of two plain concrete slabs each of dimensions 737.5 × 750 × 200 mm^3 jointed with dowels and a joint width of 25 mm, forming a specimen of size 1500 × 750 × 200 mm^3. The dimensions of the test prototypes were selected based on the experimental works on the evaluation of the performance of GFRP dowels in dowel-jointed concrete slabs-on-ground by various researchers. Al-Humeidawi and Mandal [12] tested specimens of dimensions 770 × 300 × 250 mm^3, while Li [25] and Vijay et al. [22] tested specimens of sizes 1524 × 305 × 279 mm^3. Benmokrane et al. [6] conducted experimental investigations on 2440 × 610 × 254 mm^3 specimens. The standard length of dowels according to AASHTO is 457 mm (18″) [18], which was adopted by several researchers [6,12,22,25]. The length of the stainless steel dowels used in the flood mitigation channel was 900 mm. Hence, 450 mm and 900 mm dowel lengths were chosen for the study.

The butt-joint at mid-length was created using a high-density EPS foam board with holes at the locations of dowel bars. Before testing the specimens, these foams were melted away using petrol at the casting yard and care was taken to protect the GFRP dowels from petrol. The test matrix shown as a Sankey diagram in Fig. 4 and Table 3, shows the variables such as dowel bar materials (PG, SG, and SS), dowel bar diameters (12 mm, 14 mm, 16 mm, and 38 mm), spacing of dowel bars (200 mm and 250 mm c/c), length of dowel bars (450 mm and 900 mm), type of fixity of dowel to concrete (fixed-fixed and free-fixed) and loading scheme (monotonic and cyclic). Eight specimens with GFRP dowel bars and four specimens with stainless steel dowels were cast for the experimental program. The nomenclature of specimens is as follows: the first part indicates the dowel type (PG14, SG16, PG38, or SS12), and the second part indicates the dowel length (450 mm or 900 mm). In all specimens with dowel spacing of 250 mm, the third part indicates the dowel end-fixity (F-XL, FL-X, or X-X), as shown in Fig. 5. The only specimen with 200 mm spacing was named PG14–450-200S-X-X. Vijay et al. [22], Benmokrane et al. [6], and Al-Humeidawi and Mandal [1] used fixed spacings for varying bar diameters in their experimental designs. Also, the flood mitigation channel in Jazan used a spacing of 250 mm. Thus, the authors chose 200 mm and 250 mm dowel spacings for the present study.

A suffix “CYCLIC” was added to the two specimens which were subjected to the cyclic loads. The molds for the test specimens and the slabs with doweled-joints are shown in Fig. 6. Four two-legged hooks were embedded in each specimen to transport the specimens from the casting site to the laboratory without disturbing the joint. To benchmark the load transfer performance of the doweled-joints in the specimens, the standard design wheel loads provided by AASHTO [36], listed in Table 4 were used.

2.3. Base material selection and characterization

Tests conducted on dowel-jointed slabs supported on compacted soil subbase were reported to have varying levels of modulus of subgrade reaction due to changes in the level of compaction after every test [25,26]. Thus, a suitable replacement for compacted soil subgrade was identified based on numerous trials on a variety of polystyrene foams, including various grades of expanded polystyrene (EPS) and extruded polystyrene (XPS). To investigate the modulus of subgrade reaction, foam specimens having dimensions 600 × 600 × 100 mm^3 were subjected to punching shear loads through a 200 × 200 mm^2 steel plate, as shown in Fig. 7.

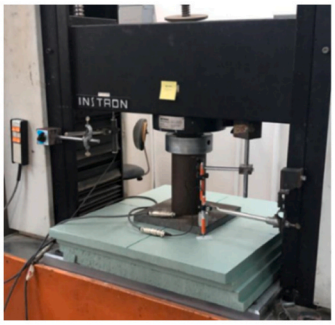

(a) Plate load test

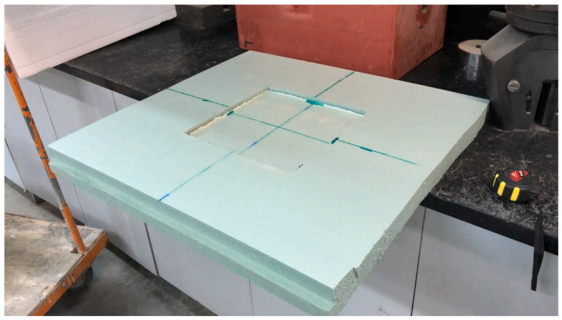

(b) failed foam specimen

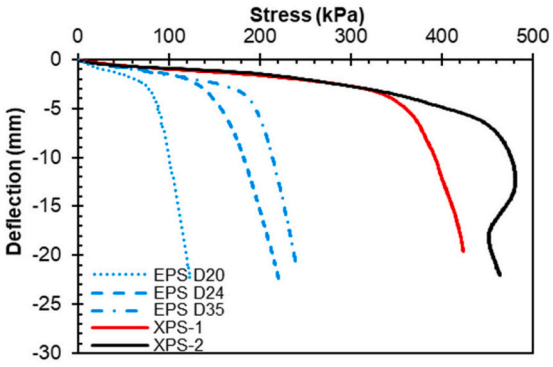

(c) Load-settlement plots of EPS and XPS foams

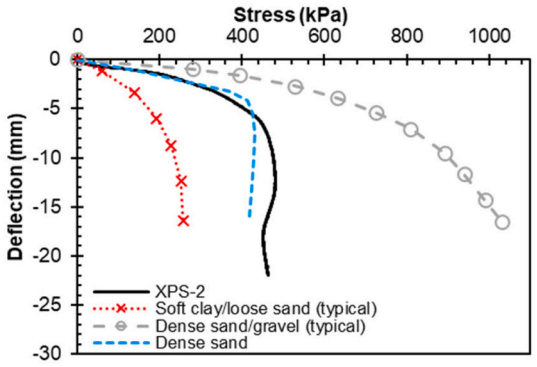

(d) Plate load tests of XPS-2, dense sand [41], and other typical soil types [42]

Fig. 7. Plate load test of extruded polystyrene foam.

Table 5
Properties of polystyrene foams.

Name	Foam type	Density (kg/m^3)	Bearing capacity (kPa)
EPS-D20	EPS	20 *	87
EPS-D24		24 *	162
EPS-D35		32-35 *	201
XPS-1	XPS	32-35 *	383
XPS-2		30.7§	480

Note: * provided by manufacturer; § determined experimentally.

The technical properties such as densities and bearing capacities of the three grades of EPS foams and two types of XPS foams are listed in Table 5. The load-settlement curves of various types of foams tested in the experimental program are plotted in Fig. 7(c). The load-bearing capacities of the foams were determined using the double-tangent method [37]. The modulus of subgrade reaction of XPS-2 was found to be approximately 124 MPa/m, which corresponds to very compacted soils such as compacted sandy clay and stiff clay, which ranges between 100 and 200 MPa/m [38] and dense sandy gravel, which varies from 100 to 150 MPa/m [39]. The load-bearing capacity of XPS-2 was observed to be approximately 480 kPa, which stands between firm to compact sand (coarse to medium) which varies from 431 kPa to 575 kPa, respectively, or between loose to firm gravel, which varies between 383 kPa and 575 kPa, respectively [40]. Fig. 7(d) presents the comparison between the plate load test results of XPS-2 with dense sand, as reported by Tabatabaei et al. [41], and dense sand or gravel and soft clay or loose sand, provided by Smith [42]. The capacity of XPS-2 was also comparable with the granular mixture prepared by Benmokrane et al. [6] to meet AASHTO Class A specifications, which achieved a subgrade modulus of 110 MPa/m. The density of XPS-2 was determined experimentally and reported in Table 5.

2.4. Test setup, instrumentation, and loading protocols

The slabs were transported carefully from the casting yard to the reaction floor in the Heavy Equipment Laboratory Building at the King Fahd University of Petroleum and Minerals (KFUPM). Extruded polystyrene foam XPS-2 of 100 mm-thickness subbase was first prepared on the reaction floor and the slab specimens were then placed on the foam. The load was applied to the slab specimens using a hydraulic jack in a loading frame as shown in Fig. 8(d). A steel column, with an axial load capacity of 1000 kN, fabricated from two steel tubes was used for the application of load from the hydraulic jack. The load was applied on one of the slabs at the edge of the joint through a 25 mm-thick steel plate of plan dimensions 200 × 200 mm^2. The 200 × 200 mm^2 loading plate was intended to represent the wheel load contact area. The plate chosen for the study provides the equivalent contact area (40,000 mm^2) of a 10 × 20 wheel which has an inflation pressure of 917 kPa and a load of 36 kN, as reported by Park [43] and De Beer et al. [44]. The concentrated load was applied mid-way along the joint on one of the two slabs, away from the slab edges, as done by other researchers [6,12,22,25]. The central loading position will give a more consistent response, avoiding the risk of non-uniformity of load application and stress concentrations from loads at the edge, which may overshadow the effect of parameters investigated in the study. The instrumentation for measuring the response of the joint included 16 LVDTs, strain gauges, and a load cell. Vertical displacements at 16 points on the top surface of the specimens (Fig. 8(a)) were monitored using linear variable differential transducers (LVDT) along with the corresponding load carried by the specimen using a load cell of 1000 kN capacity. LVDTs at L1 to L6 and R1 to R6 were used to plot profiles of vertical displacements at a particular load, while L3, LM1, RM1, and R3 measured the loaded slab displacements, and L4, LM2, RM2, and R4 measured unloaded slab displacements at the joint edges. The load cell was installed above the hydraulic jack with a load capacity of 1000 kN, resting on top of the

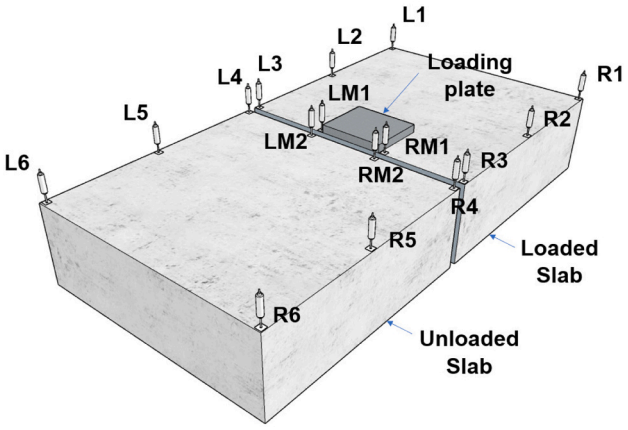

(a) Schematic of LVDT instrumentation

(b) LVDT at joint

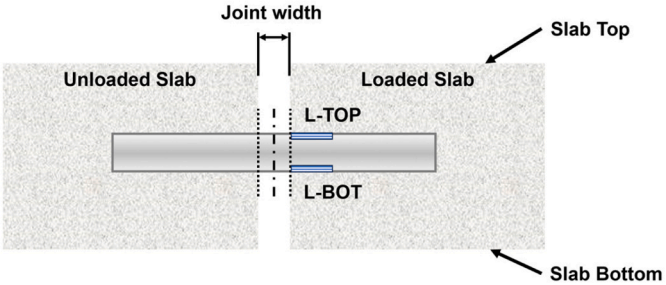

(c) Strain gauges on the dowel bars

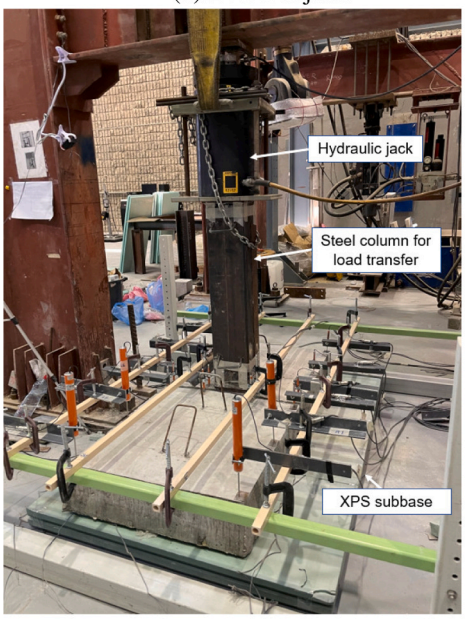

(d) loaded specimen

Fig. 8. Load test of slab specimen with doweled-joint resting on XPS-2 subbase.

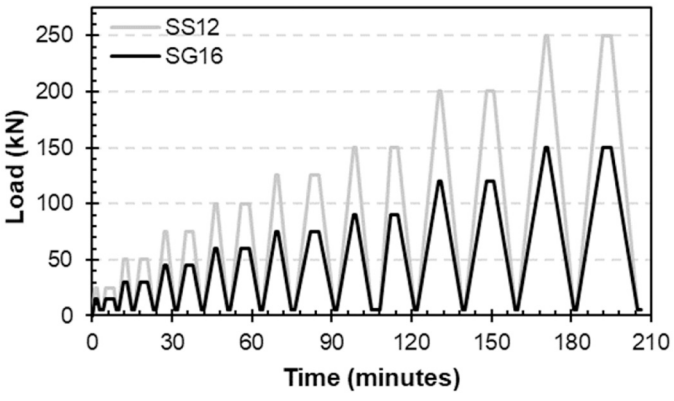

Fig. 9. Cyclic loading protocol used in the study.

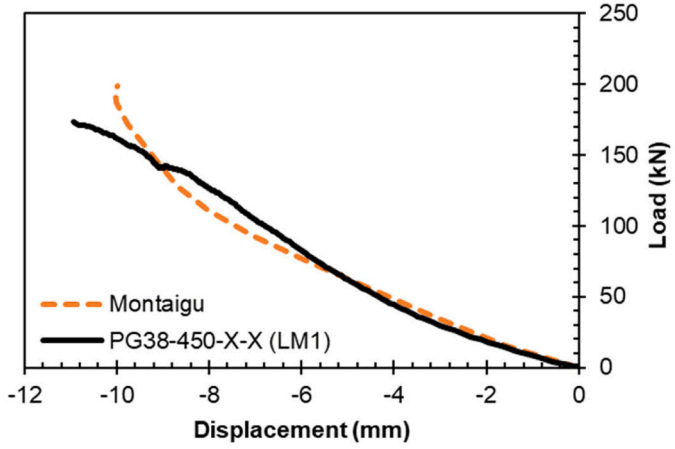

Fig. 10. Load-displacement curves of PG38–450-X-X compared with results from Montaigu [26].

loading steel column. A special frame made of GFRP tube sections was fabricated and placed over the specimens, as shown in Fig. 8(d). To monitor strains in the dowel bars, strain gauges were installed on the top (L-TOP) and bottom (L-BOT) surfaces of the dowel bars embedded in the loaded slabs of the specimens, as shown schematically in Fig. 8(c).

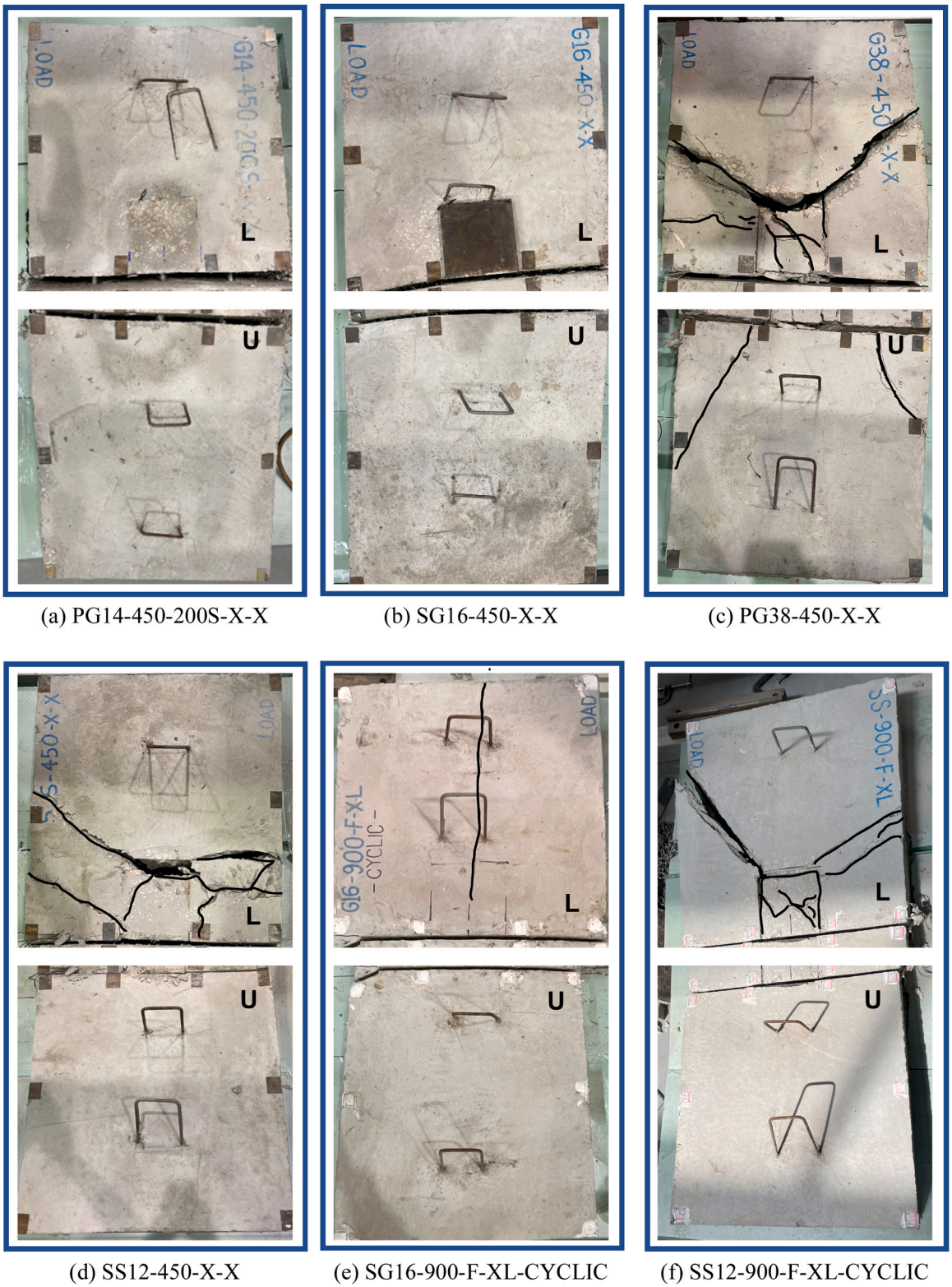

Fig. 11. Specimen failure modes (L: loaded slab; and U: unloaded slab).

The monotonic loads were applied at a rate of approximately 2 mm/min, while the cyclic loads were applied based on the loading protocol shown in Fig. 9, devised based on in-situ and laboratory cyclic experiments in the literature [45–50] since a standardized loading protocol for laboratory tests was not available. The one-way cyclic loading scheme consisted of increasing values of loads every two cycles of load application and removal. The load level at each increment was applied twice with 1-minute and 3-minute durations before increasing the peak for the subsequent cycles. Based on expected failure loads of 250 kN in the SS12 dowel-jointed slab specimen, and 150 kN in the SG16 dowel-jointed slab specimens, initial and increment loads of 25 kN and 15 kN were chosen in SS12 and SG16 dowel-jointed slab specimens, corresponding to 10% of their ultimate loads, respectively. Beyond the expected peak load, loading was continued until failure. The minimum load in the protocol

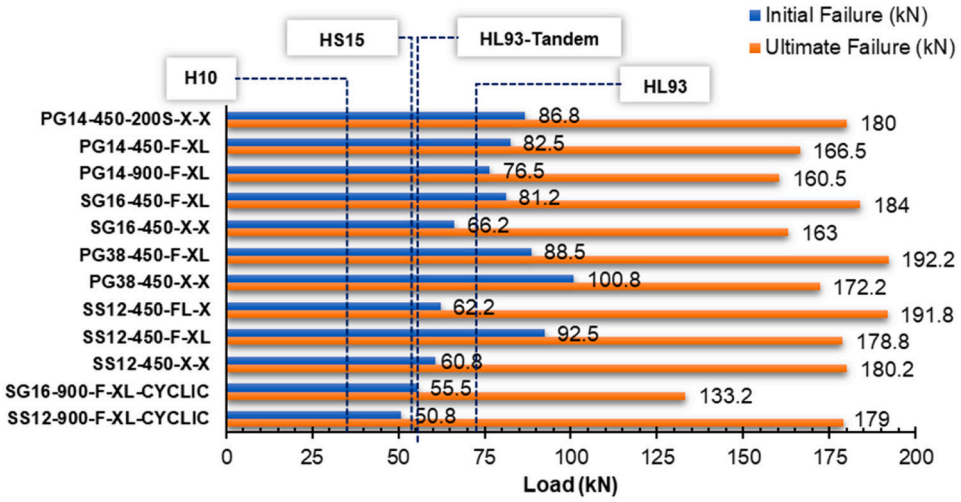

Fig. 12. Initial and ultimate failure load capacities of specimens.

was chosen as 5 kN to maintain the action of the hydraulic jack. The total duration of cyclic loading was approximately 3.5 h.

3. Results and discussion

3.1. Validation of XPS-2 representing soil

To validate the response of XPS-2 under load as a simulated subbase replacing soil, results from tests conducted on a specimen with 38 mm-diameter dowel bars were compared with the experimental results reported by Montaigu [26] in a test to investigate the performance of a dowel-jointed slab of dimension 2440 × 610 × 254 mm^3, with two 38 mm-diameter GFRP dowels of 460 mm length, spaced at 306 mm center-to-center. A granular mixture adhering to AASHTO Class A specifications was prepared using 50% (0–5 mm) sand, 20% (10 mm) crushed rock, and 30% (20 mm) crushed rock aggregates, to achieve a subgrade modulus of 110 MPa/m using a Briaude Compacting Device. The deflection of the loaded slab near the joint was compared with the results from tests conducted in the present work on PG38–450-X-X, as shown in Fig. 10. The close match in the load-displacement responses between the experimental works conducted on compacted soil and the XPS-2 subbase used in this study shows that XPS-2 is a suitable replacement to compacted soil.

3.2. Modes of failure and crack patterns

The mode of failure of the dowel bars used in the experimental program varied significantly depending on the bar diameter. The development and generation of cracks in the concrete slab also depend on the bar diameter. Top views of some of the specimens after failure are presented in Fig. 11. It may be noted from the figure that failure in dowel-jointed slabs with smaller diameter GFRP dowel bars (PG14 and SG16) was mostly governed by the shear failure of the GFRP dowels, unlike the case of the slabs with the larger diameter dowel (PG38), and the stainless steel dowel (SS12). In all slabs with PG14 and SG16 dowels with 250 mm spacing, no apparent cracks in concrete were observed. However, in PG14–450-200S-X-X, the only PG14 slab with 200 mm spacing, a crack was developed near the central dowel bar, parallel to the direction of the dowels (see Fig. 11 (a)). Slabs with PG38 and SS12 dowels exhibited extensive damage in concrete, as shown in Fig. 11 (c and d). When subjected to cyclic loads, the PG14 doweled specimen PG14–900-F-XL-CYCLIC, exhibited a single crack running in the longitudinal direction of the specimen from the central dowel in the loaded slab, as shown in Fig. 11 (e), and SS12 doweled specimen SS12–900-F-XL-CYCLIC developed two major cracks on the loaded slab. The initial failure (representing the first change in slope in the load-deflection response) and the ultimate failure (representing failure of dowels or concrete failure or combined failure) loads in all specimens plotted in Fig. 12 were compared with the design wheel loads H10 (~35.6 kN), HS15 (~53.4 kN), HL93-tandem (~55.6 kN), and HL93 (~72.5 kN), specified by AASHTO [18]. All 12 specimens exhibited their initial failure at a load significantly higher than the H10 design wheel load.

3.3. Effect of various parameters on load-deflection response and failure

3.3.1. Effect of dowel diameter and material type

Specimens PG14–450-F-XL (14 mm dowel bar) and PG-38–450-F-XL (38 mm dowel bar) were used to compare the effect of bar diameter on the performance of dowels. The reinforcement ratios per dowel bar for the 14 mm and 38 mm dowels were calculated to be 0.31% and 2.27%, respectively. The initial and ultimate failure loads in the PG14 specimen were 82.5 kN and 166.5 kN, which were 6.8% and 13.4% lesser than the corresponding values in the PG-38–450-F-XL (Fig. 12). The increase in reinforcement ratio from 0.31% to 2.27% increased the ultimate load capacity from 166.5 kN to 192.2 kN. Although the cracking and failure loads were not very different from each other, the modes of failure in these dowel-jointed slabs were significantly different. The failure in the PG14–450-F-XL slab, shown in Fig. 13 (a and b), was characterized by the shear failure of the GFRP dowels without any damage in the concrete slabs. However, on the other hand, the failure in PG38–450-F-XL was characterized by extensive damage to concrete with no noticeable failure in the 38 mm-diameter GFRP dowel (Fig. 13 (c and d)). The load-displacement curves shown in Fig. 14 (a) show that the PG38 slab exhibited slightly higher stiffness and strength until failure compared to the PG14 specimen. At a load of 35.6 kN, the relative deflections in PG14–450-F-XL and PG38–450-F-XL were calculated to be 2.52 mm and 0.78 mm, respectively (Fig. 14 (b)). When comparing the load transfer performance of the specimens, the PG38–450-F-XL was more efficient in transferring the applied loads between the joints. The joint effectiveness (E) and load transfer efficiency (LTE) of the specimens are presented in Fig. 14 (c and d), respectively. At 35.6 kN, E and LTE of PG38–450-F-XL are 84.9% and 73.7%, respectively as compared to 87.1% and 77.1% in PG14–450-F-XL, and 97.0% and 94.2% in SG16–450-F-XL, calculated based on the vertical displacements near the joint (Table 6). Both specimens with smaller diameter dowel bars exhibited slightly better E and LTE values as compared to the larger diameter dowel bars. While SG16–450-F-XL maintained this performance up to larger loads, PG14–450-F-XL performed satisfactorily up to 60 kN, beyond which the E and LTE dropped. The vertical deflection profiles in longitudinal and lateral directions of the specimens at the H10 design wheel load

(a) PG14-450-F-XL: unloaded slab after failure

(b) PG-14 dowel failed in shear

(c) PG38-450-F-XL: loaded slab

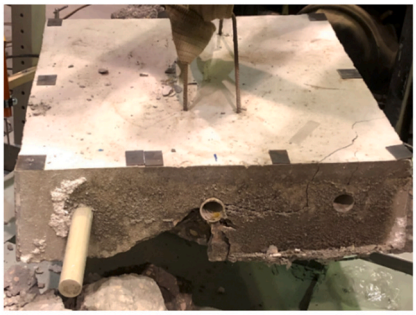

(d) PG38-450-F-XL: unloaded slab

(e) shear failure in SG16 dowel bar

(f) SS12-450-F-XL: failure in loaded slab

(g) yielded SS12 dowel bar

(h) PG14-450-200S-X-X: loaded slab

Fig. 13. Failure in specimens under monotonic loads.

(~35.6 kN) are presented in Fig. 14 (e). The vertical deflection in PG14–450-F-XL on the loaded side of the joint is 11.3 mm, as compared to 7.1 mm in SG16–450-F-XL and 3.0 mm in PG38–450-F-XL. At the end of the unloaded slab, the uplifts in PG14–450-F-XL, SG16–450-F-XL, and PG38–450-F-XL were 16.8 mm, 0.7 mm, and 0.4 mm, respectively. The lower shear capacity and flexural rigidity of PG14 dowels are the causes of the large deflection at joints and uplift at the ends. It can be noted here that SG16 exhibited a performance comparable with the PG38 dowels, in terms of deflections and load transfer characteristics.

To compare the effect of dowel materials, GFRP dowels (SG16) of 16 mm dia. and stainless steel dowels (SS12) of 12 mm dia. of comparable flexural rigidity (*EI*) were used for analysis, in specimens SG16–450-F-XL and SS12–450-F-XL, respectively. The initial failure loads in SG16–450-F-XL and SS12–450-F-XL were observed to be 81.2 kN and 92.5 kN, respectively, while the ultimate loads were noted to be 184 kN and 178.8 kN. The larger deflections in SG16–450-F-XL, as compared to SS12–450-F-XL at any given load is due to the lower shear modulus of GFRP bars, which is approximately 3.5 GPa [6,12] as compared to stainless steel which has a minimum shear modulus of 74 GPa in AISI 316, which is most commonly used for marine environments [6,51].

The mode of failure in SG16–450-F-XL involved no cracking in

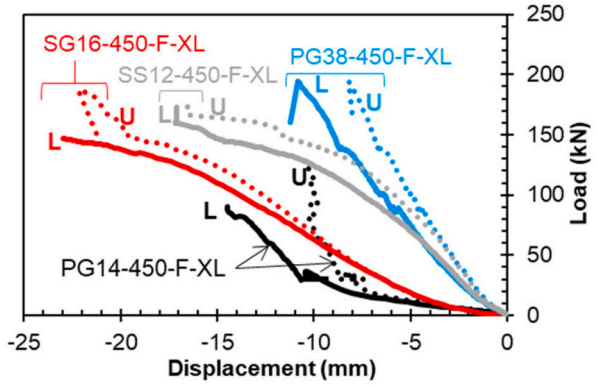

a) Load-deflection plot in dowel-jointed slab specimens at LM1 and LM2 (L: loaded slab; and U: unloaded slab)

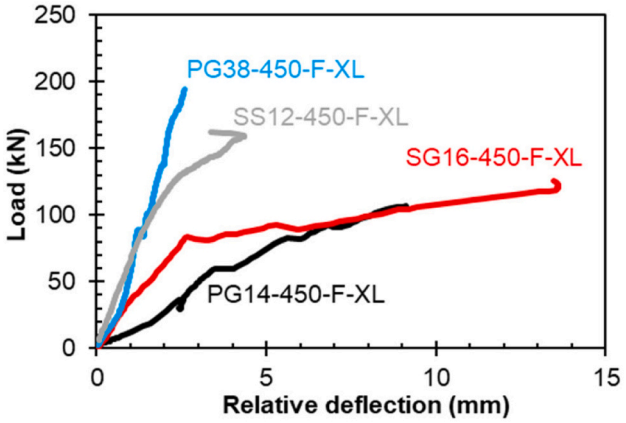

(b) relative deflections

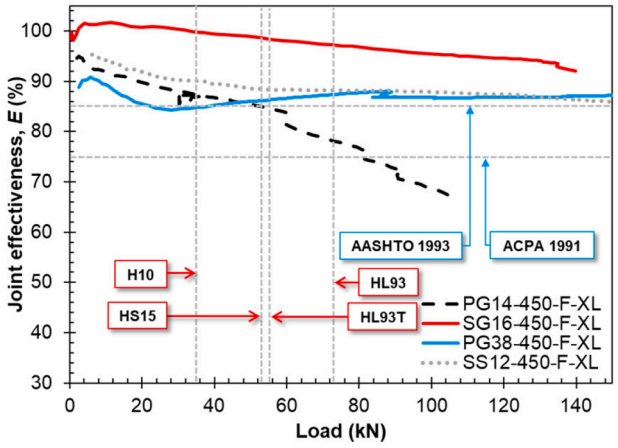

(c) joint effectiveness, *E*

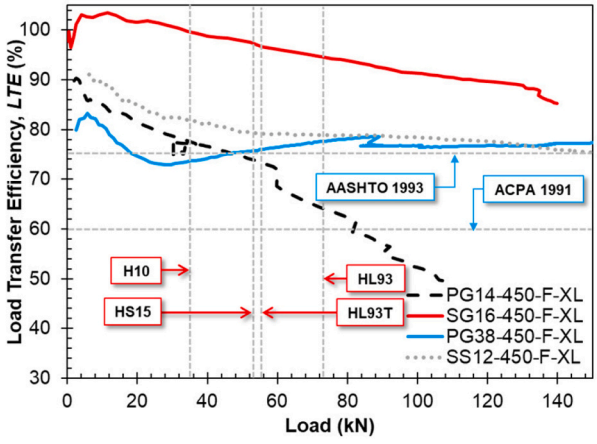

(d) load transfer efficiency, *LTE*

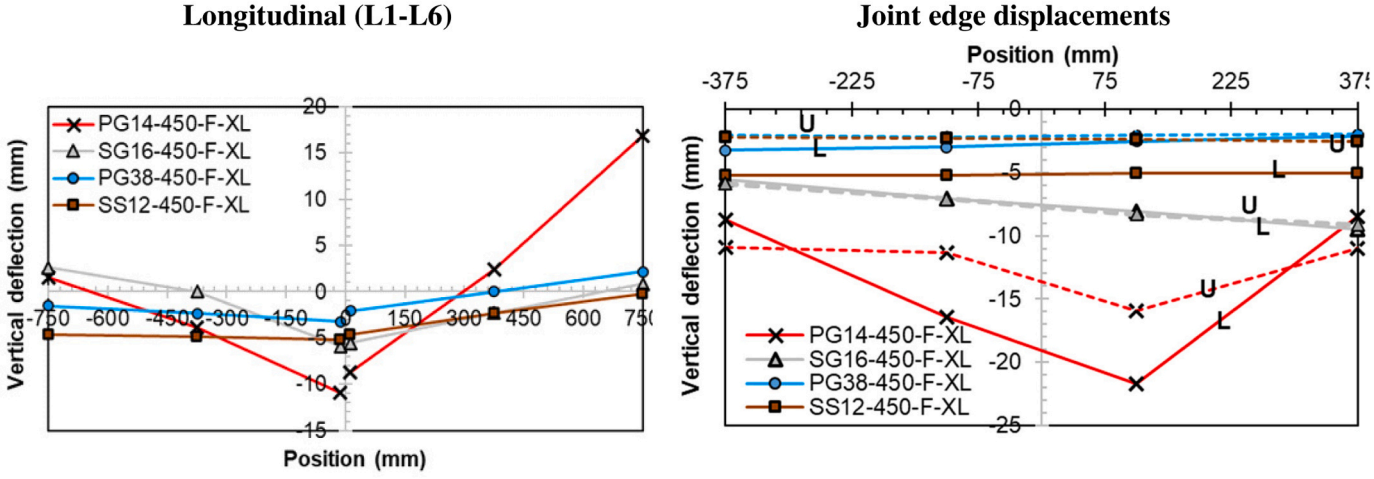

(e) vertical deflection profile at H10 (~35.6 kN) (L: loaded slab; and U: unloaded slab)

Fig. 14. Effect of dowel bar diameter and material type.

Table 6
Effect of dowel bar diameter and material type on E, LTE and relative deflection at 35.6 kN load.

Specimen ID	Loaded slab, δ_l (mm)	Unloaded slab, δ_u (mm)	Joint effectiveness, *E* (%)	Load transfer efficiency, *LTE* (%)	Relative deflection, Δ (mm)
PG14-450-F-XL	11.00	8.48	87.1	77.1	2.52
SG16-450-F-XL	5.86	5.52	97	94.2	0.34
PG38-450-F-XL	2.97	2.19	84.9	73.7	0.78
SS12-450-F-XL	2.80	2.29	90	81.8	0.51

concrete, similar to PG14–450-F-XL, where failure was controlled by the shear failure of the GFRP dowel bars (Fig. 13 (e)). In the case of SS12–450-F-XL, extensive cracking in the loaded concrete slab was observed which was parallel to the plane of the joint at the ends of the embedded dowel bar and along a plane perpendicular to the plane of the joint, as shown in Fig. 13 (f). All three 12 mm-diameter stainless steel dowels (SS12) yielded at failure loads with large deformations, accompanied by concrete bearing failure (Fig. 13 (g)). Both dowel-jointed slab specimens were found to transfer loads considerably well beyond the AASTHO and ACPA limits. At HL93 design wheel load of 71.2 kN, the joint effectiveness (*E*) values in SG16–450-F-XL and SS12–450-F-XL were calculated to be 94.1% and 93.3%, respectively, while the load transfer efficiency (*LTE*) values were found to be 88.9% and 87.4%, respectively (Fig. 14 (c and d)). The vertical deflection profiles in both specimens were approximately similar, across the joint along L1-L6 (Fig. 14 (e)). At a lower load of H10, the *E* and *LTE* values indicate that both SS12 and SG16 bars could have been used in the Jazan flood mitigation channel, where only the SS12 dowels were used [29]. Thus, it can be concluded that SG16 dowel bars are a suitable alternative to SS12 dowels in slabs-on-ground with doweled-joints in industrial facilities, flood mitigation channels, walkways, and parking lots.

For PG14 and SG16 dowel bars, the bearing stress equation (Eq. 4) yielded values of approximately 84.8 MPa and 65.3 MPa, respectively, which are significantly higher than the concrete permissible bearing stress (f_b) of 45.8 MPa, in the present study. It was observed from Fig. 11 and Fig. 13 that failure from bearing was observed only in PG38 and SS12 dowels, while failure in PG14 and SG16 specimens was associated with shear failure of bars, without any damage in concrete from bearing stresses. Since the shear capacity of the GFRP is less compared to steel, and cross-section of the bar is more susceptible to geometric instabilities under shear loads and the development of bearing stresses in the concrete is not critical, most of the strain energy is dissipated due to the shear deformation of the bar. The equation for predicting bearing stress (Eq. 6) from the dowels is valid for bars with larger diameters or with a higher stiffness.

The experimental results indicate that, for smaller diameter GFRP dowel bars, the design of the joint is not governed by the bearing stresses developed in the concrete at the joint, which raises the need for the development of a numerical model, validated by appropriate experimental results to suggest pavement dowel design modifications for the application to GFRP dowel bars in jointed rigid pavements.

3.3.2. Effect of dowel spacing

The spacings between the dowels play an important role in the ability of dowels to transfer loads laterally as the effective number of dowels participating in load transfer increases [6]. Two different spacings of PG14 dowels, 200 mm and 250 mm, with the reinforcement ratios per dowel bar of 0.38% and 0.31%, respectively were used to investigate the effect of GFRP dowel bar spacings. The closer spacing of dowel bars (higher reinforcement ratio per dowel bar) in PG14–450-200S-X-X resulted in slightly higher initial and ultimate failure loads of 86.8 kN and 180 kN, respectively, which is approximately 5.2% and 8.1% higher than the corresponding loads in PG14–450-F-XL (initial: 82.5 kN; ultimate: 166.5 kN). The smaller spacing of dowels (200 mm c/c) also resulted in a different mode of failure which involved the cracking of loaded concrete slab, as shown in Fig. 13 (h), unlike PG14–450-F-XL which involved only the shear failure of dowel bars without any apparent damage in concrete. However, no bearing failure of concrete at the joint face was observed (Fig. 13 (h)). The load transfer characteristics of PG14–450-200S-X-X were also found to have improved with a smaller dowel spacing. The joint effectiveness (*E*) and load transfer efficiency (*LTE*) was found to be 94.5% and 89.6%, respectively in PG14–450-200S-X-X, as compared to 87.1% and 77.1% in PG14–450-F-XL, at a load of 35.6 kN, which corresponds to H10 design wheel load (Fig. 15 (c and d) and Table 7). The load transfer efficiency is significantly increased when the number of effective dowel bars under the wheel load increases for 200 mm c/c spacing. At the same load, the relative deflection in PG14–450-200S-X-X was as low as 0.49 mm, as compared to 2.52 mm in PG14–450-F-XL. At a higher design wheel load of HS15 (~53.4 kN),10 H *E* and *LTE* in PG14–450-200S-X-X were 92.6% and 86.2%, respectively, as compared to 87.8% and 78.0%, respectively in PG14–450-F-XL. This ensures that PG14–450-200S-X-X would offer better riding comfort and minimal damage to concrete. The vertical displacement profiles (longitudinal and transverse) of the specimens at 35.6 kN, shown in Fig. 15 (e), indicate large reductions in deflections in PG14–450-200S-X-X as compared to PG14–450-F-XL, in longitudinal and transverse directions.

The significantly higher *E* and *LTE* at a lower spacing indicate that GFRP bars could be effectively used in slabs-on-ground. It is evident from the values of *E* and *LTE* that these small-diameter GFRP dowels have a strong potential for various applications where only low concentrated loads are expected.

3.3.3. Effect of dowel length

The effect of embedment length on smaller diameter GFRP dowel bars was investigated in the study. The GFRP dowel specimen with 900 mm embedment length, PG14–900-F-XL was compared with the load-displacement and load transfer characteristics of PG14–450-F-XL with 450 mm dowel length. The load-displacement plots indicate that there was a significant increase in the stiffness of the joint upon increasing the length of the 14 mm-diameter dowels, as shown in Fig. 15 (a). There was, however, no difference in the mode of failure of the specimens, which was characterized by the failure of the GFRP dowels without cracking in concrete.

Although at any given load the absolute displacements and relative deflections in the PG14–900-F-XL were much lower, and relative deflections (Fig. 15 (a and b)) were lower than PG14–450-F-XL, the load transfer performance values in terms of joint effectiveness (*E*) and load transfer efficiency (*LTE*) were lesser. This is because both *E* and *LTE* are ratios of deflections in the loaded and unloaded slabs. At 35.6 kN, *E* and *LTE* values of PG14–900-F-XL were 80.0% and 66.6%, respectively, as compared to 87.1% and 77.1% in PG14–450-F-XL (Fig. 15 (c and d) and Table 7). While PG14–900-F-XL does not qualify for the AASHTO (1993) requirements, it satisfies the less stringent ACPA (1991) limits of *E* (75%) and *LTE* (60%). At 35.6 kN, the relative deflection in PG14–900-F-XL was 1.16 mm. The profiles of vertical displacements along the length and across the joint of the specimens at 35.6 kN show that PG14–900-F-XL has lower deflection as compared to PG14–450-F-XL (Fig. 15 (e)).

3.3.4. Effect of dowel end-fixity

In field applications, GFRP dowels are not always provided with bond-breakers in the concrete-embedded part of the dowel, since GFRP dowel bars are very smooth and the development of expansive corrosion

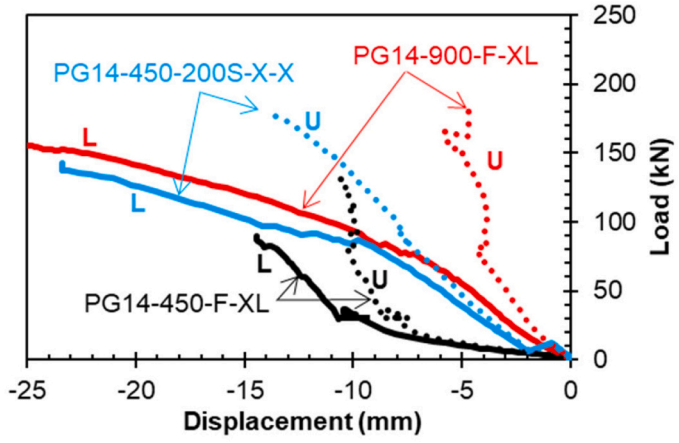

(a) Load-deflection plot in dowelled slab specimens at LM1 and LM2 (L: loaded slab; and U: unloaded slab)

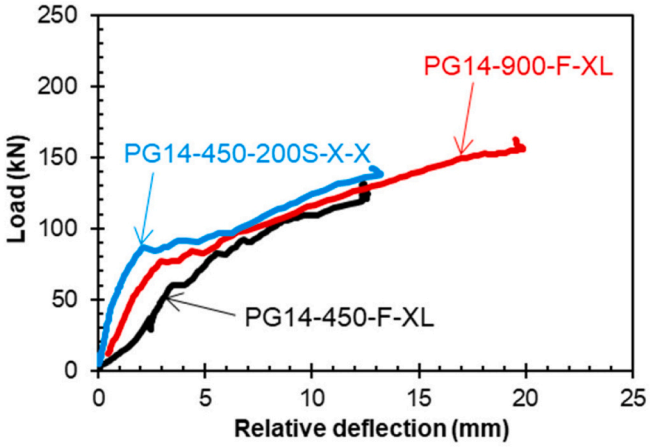

(b) relative deflection

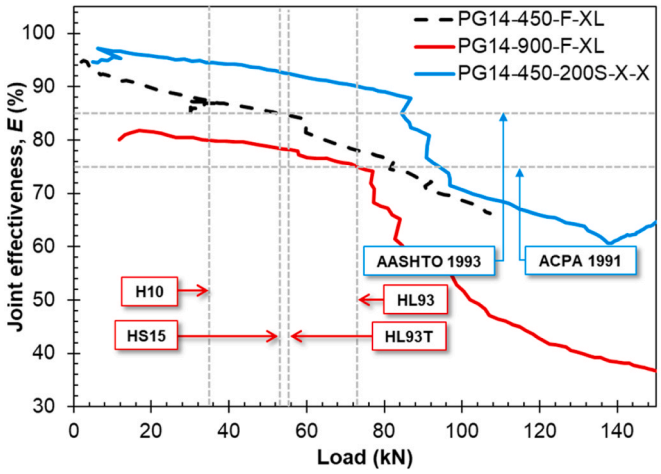

(c) joint effectiveness, *E*

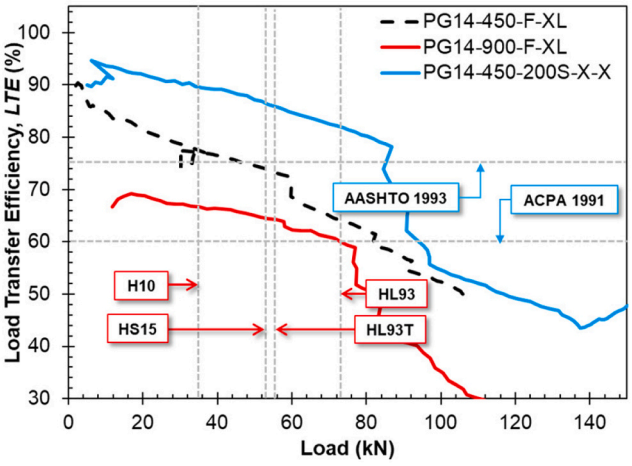

(d) load transfer efficiency, *LTE*

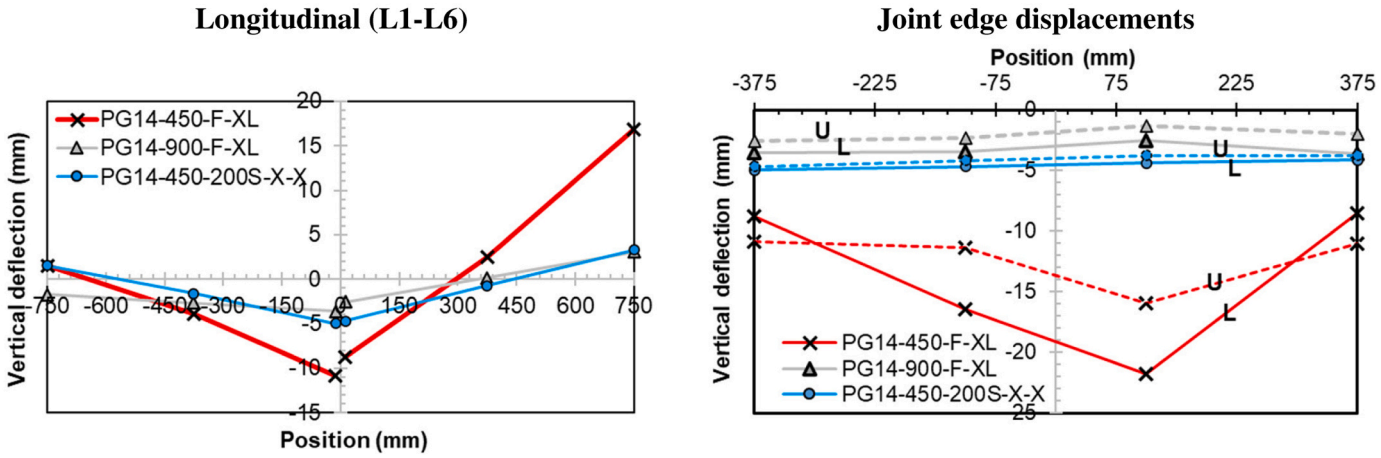

(e) vertical deflection profile at H10 design wheel load (~35.6 kN)

Fig. 15. Effect of dowel length and spacing.

products is not expected, unlike steel dowels. However, the provision of a bond-breaker and looseness in dowels creates a very different mechanical boundary condition (Fig. 5(a and b)) as compared to a fixed-fixed condition, as shown in Fig. 5(c). A notable effect on the load-displacement and load transfer characteristics in slabs was observed when the dowel end-fixities were varied.

Comparisons of the effect of dowel end-fixity on the load-displacement curves on either side of the joint, are plotted in Fig. 16 (a and c). Among the seven dowel-jointed slabs compared, it was found that the dowel-end fixity condition F-XL had significantly lesser

Table 7
Effect of dowel length and spacing on E, LTE and relative deflection at 35.6 kN load.

Specimen ID	Loaded slab, δ_l (mm)	Unloaded slab, δ_u (mm)	Joint effectiveness, *E* (%)	Load transfer efficiency, *LTE* (%)	Relative deflection, Δ (mm)
PG14-450-F-XL	11.00	8.48	87.1	77.1	2.52
PG14-900-F-XL	3.47	2.31	80.0	66.6	1.16
PG14-450-200S-X-X	4.71	4.22	84.5	89.6	0.49

displacements in most cases. For instance, for a load of 71.2 kN, corresponding to the HL 93 design truck wheel load at LVDT location LM1 (loaded slab deflection near joint), in SG16–450-F-XL (specimen with fixed-free end condition of SG16 dowels with load acting on fixed end of the dowel), vertical displacement on the loaded slab was 20.0% lesser than the corresponding displacement in SG16–450-X-X (specimen with fixed-fixed end conditions of SG16 dowels). In PG38–450-F-XL, LM1 displacements were 21.7% lower than the corresponding displacements in PG38–450-X-X. Also, in the case of slabs with stainless steel dowels, LM1 displacements in SS12–450-F-XL (specimen with fixed-free end-condition of SS12 dowels with load acting on fixed end of the dowel) were 23.6% and 49.1% lesser than the corresponding displacements in SS12–450-X-X (fixed-fixed dowel end-conditions) and SS12–450-FL-X (free-fixed dowel end-conditions with load acting on the free side), respectively for HL 93 design truck wheel load. The load transfer characteristics, in terms of *E* and *LTE* of SG16 dowel-jointed slabs (Fig. 16 (e and f)) show that the X-X dowel-end fixity exhibited high efficiencies with 91.1% and 83.7% at 35.6 kN (Table 8). Beyond 45 kN, the values of *E* and *LTE* were found to decline. These values, however, were acceptable according to ACPA 1991 norms, up to HL93 design tandem truck wheel loads (~55.6 kN). In PG38–450-F-XL and SS-450-F-XL, the load transfer characteristics were on par with their counterparts with X-X dowel end-fixity. No variations in relative deflections were observed in the three comparisons. In all three comparisons, up to approximately 75 kN load, no apparent differences could be identified. At 35.6 kN, the relative deflections were 0.34 mm, 0.65 mm, 0.78 mm, and 0.18 mm in SG16–450-F-XL, SG16–450-X-X, PG38–450-F-XL, and PG38–450-X-X, respectively (Table 8). The vertical displacement profiles in the longitudinal direction of the specimen and along the edges of the joints of the specimens at 35.6 kN load are plotted in Fig. 16 (g and h), respectively. Specimens with PG38 dowels, namely PG38–450-F-XL and PG38–450-X-X, in general, exhibited lower deflections as compared to SG16–450-F-XL and SG16–450-X-X. In specimens with SS12 dowels, specimens with F-XL and X-X exhibited lower deflections as compared to FL-X by approximately 54% (Fig. 5).

3.3.5. Response under cyclic loading

To study the cyclic load response of GFRP and stainless steel dowel-jointed slabs, two slabs were subjected to cyclic loading schemes as shown in Fig. 9. The load-displacement responses, the joint load transfer characteristics, and relative deflections in GFRP and stainless steel dowel-jointed slabs specimens, namely SG16–900-F-XL-CYCLIC and SS-900-F-XL-CYCLIC, respectively are compared in Figs. 17 and 18.

The initial failure loads in the specimens subjected to cyclic loads with SG16 and SS12 were observed to be 55.5 kN and 50.8 kN, respectively, while the ultimate load capacities were recorded to be 133.2 kN and 179.0 kN. The load-displacement curves (Fig. 17 (a)) show that, at loads up to 9 kN, the SG16 GFRP dowel exhibited a mildly stiffer response as compared to the stainless steel (SS) dowel-jointed slab in the loaded slab. In the unloaded slabs, the specimen with SG16 did not exceed the displacements beyond 6 mm, even at loads of approximately 130 kN. This is due to the initial failure in the SG16 specimen, probably caused by the initiation of shear failure of the glass fibers. The effect of the initial failure is also reflected in the comparison of relative deflections of the specimens with SG16 and SS12 dowel bars. This resulted in larger relative deflections in specimens with SG16 as compared to SS12 dowel-jointed slabs at loads beyond 60 kN (Fig. 18 (a)). The cyclic load specimens with SG16 and SS12 dowels are compared with the load-displacement responses from SG16–900-F-XL and SS12–450-F-XL, respectively, which were subjected to monotonic loads (Fig. 17 (b and c)). The load transfer characteristics in the GFRP dowel-jointed slab were found to reduce after every cycle (Fig. 18), beyond the initial failure load of 55.5 kN. With the progression of every cycle, the *E* was found to degrade from an initial value of 92.5% to 88.9%, 84.7%, 82.8%, 67.48%, 52.5%, and 37.48% at the end of 2^{nd}, 4^{th}, 6^{th}, 8^{th}, 10^{th}, and 12^{th} cycles, respectively. A proportional trend was also observed in the degradation of *LTE* values, rendering an unsatisfactory response as per AASHTO and ACPA recommendations. In stainless steel dowel-jointed slab, SS-900-F-XL-CYC, the joint effectiveness (*E*) was found to degrade from an initial value of 96.3% to 93.4%, 93.0%, 90.9%, 87.7%, 84.2%, and 80.0% after 2^{nd}, 4^{th}, 6^{th}, 8^{th}, 10^{th}, and 12^{th} cycles, respectively. Although, the specimen SS12–900-F-XL-CYC failed to satisfy the AASHTO limits of *E* and *LTE* at higher loads after the 6^{th} cycle, the ACPA conditions of *E* and *LTE* were satisfied. This indicates that until the initial load capacity of the SG16 GFRP doweled specimen, the load transfer efficiencies were within the ACPA limits,

3.4. Strains in dowel bars

Strains in dowel bars at L-TOP and L-BOT locations in seven representative specimens from the 12 specimens were plotted in Fig. 19. Since L-TOP and L-BOT were located at diametrically opposite points in the dowels in the longitudinal direction, strains at these locations were found to be symmetric, with L-BOT recording tensile strains and L-TOP recording compressive strains. It can be observed from the figure that the PG38 dowel exhibited the least strains, followed by SS12, SG16, and PG14 in the specimens with 250 mm c/c, as expected. The specimen with 200 mm c/c spacing (PG14–450-200S-X-X), exhibited significantly lower strains as compared to the 250 mm spacing specimen, PG14–450-F-XL. Strains in the dowel-jointed slabs subjected to cyclic loads were only available until approximately 40 kN, beyond which the strain gauges were not functioning.

4. Conclusions

An experimental work was conducted to study the load transfer across a transverse joint between adjacent concrete slabs-on-ground by smaller diameter GFRP dowel bars. The performance of GFRP dowel types, diameter, spacings, and embedment lengths was investigated by conducting load tests on 12 dowel-jointed slabs resting on an extruded polystyrene (XPS) simulated subbase. The following conclusions were drawn from load tests conducted in the study:

- For the large diameter GFRP and steel dowels used in highway pavements, the modulus of dowel support (bearing stress in concrete) is the principal mechanism of load transfer, and failure results when the bearing stress of dowels exceeds the allowable bearing stress of concrete. The failure is dominated by cracking in concrete. For smaller diameter GFRP dowel bars, however, the bearing stresses are low and the high tensile strength of the embedded glass fibers plays a dominant role in the load transfer. The failure in the GFRP dowel bars takes place due to shear in the transverse direction since the shear capacity is low.

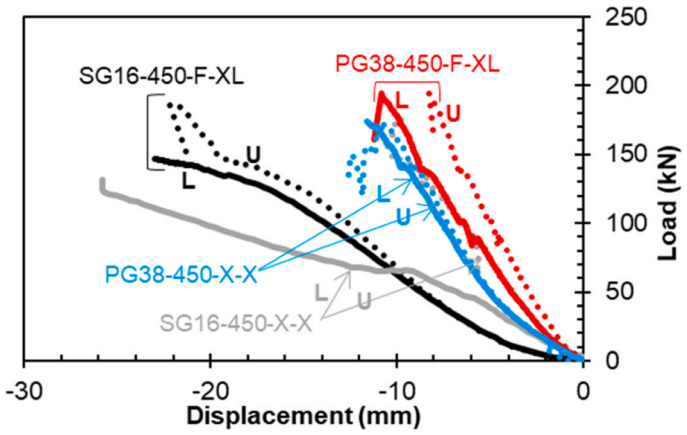

(a) Load-deflection plot in dowel-jointed slab specimens at LM1 and LM2 (L: loaded slab; and U: unloaded slab) – GFRP dowel-jointed slabs

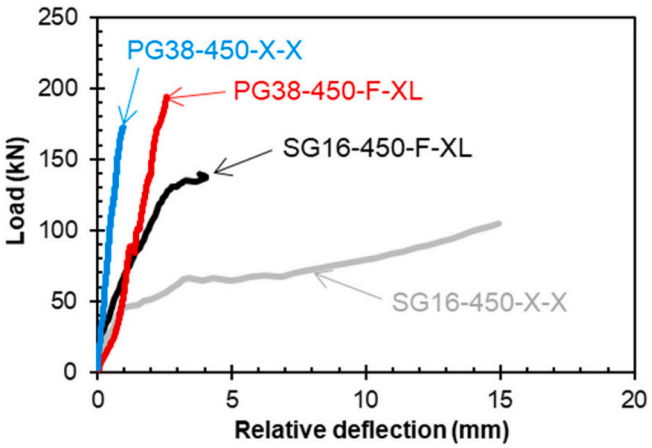

(b) relative deflection (GFRP dowel-jointed slabs)

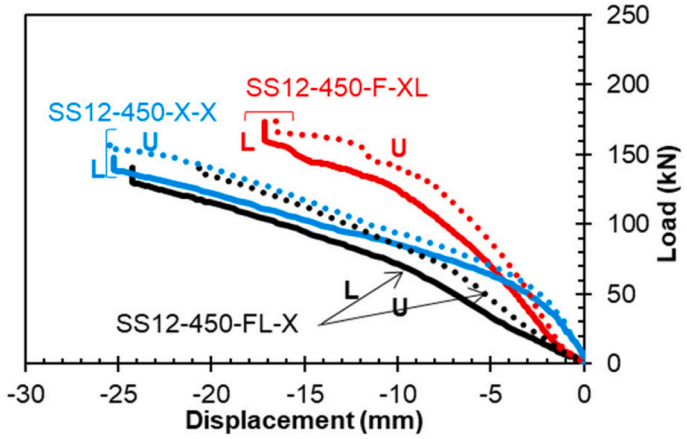

(c) Load-deflection plot in dowel-jointed slab specimens at LM1 and LM2 (L: loaded slab; and U: unloaded slab) – SS dowel-jointed slabs

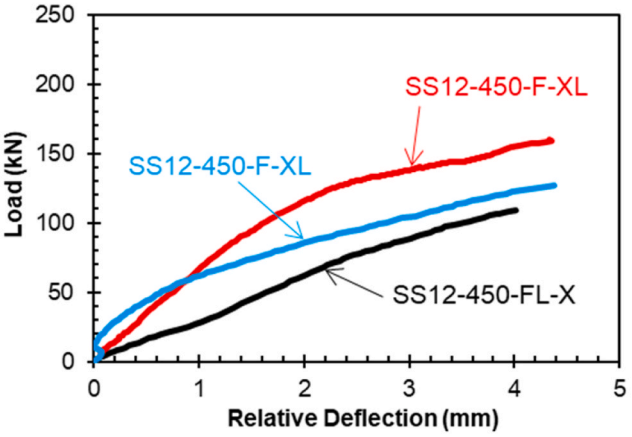

(d) relative deflection (SS dowel-jointed slabs)

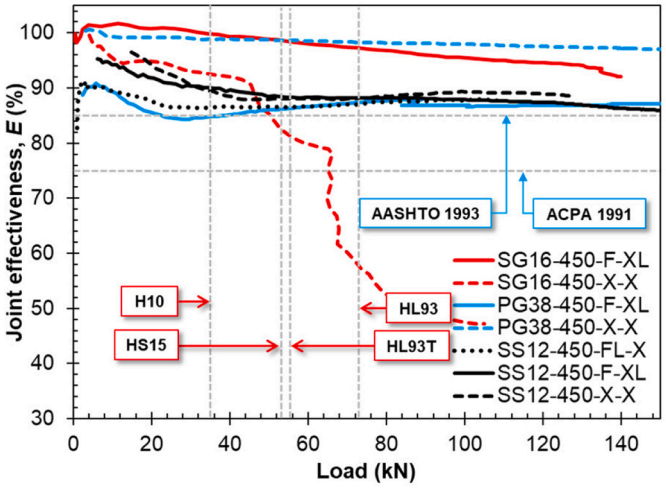

(e) joint effectiveness, *E*

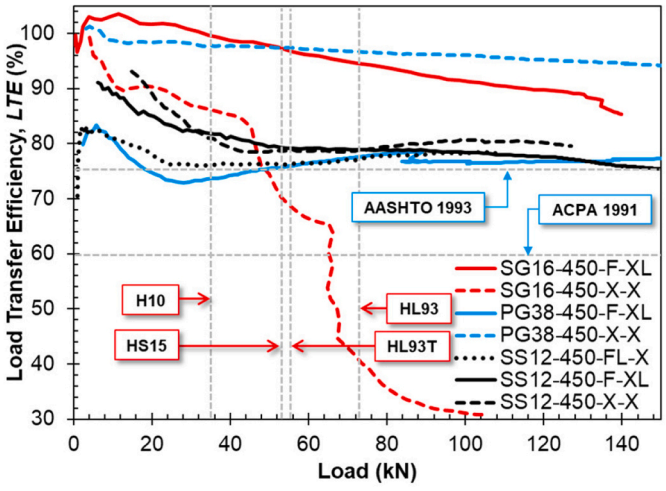

(f) load transfer efficiency, *LTE*

Fig. 16. Effect of dowel-end fixity

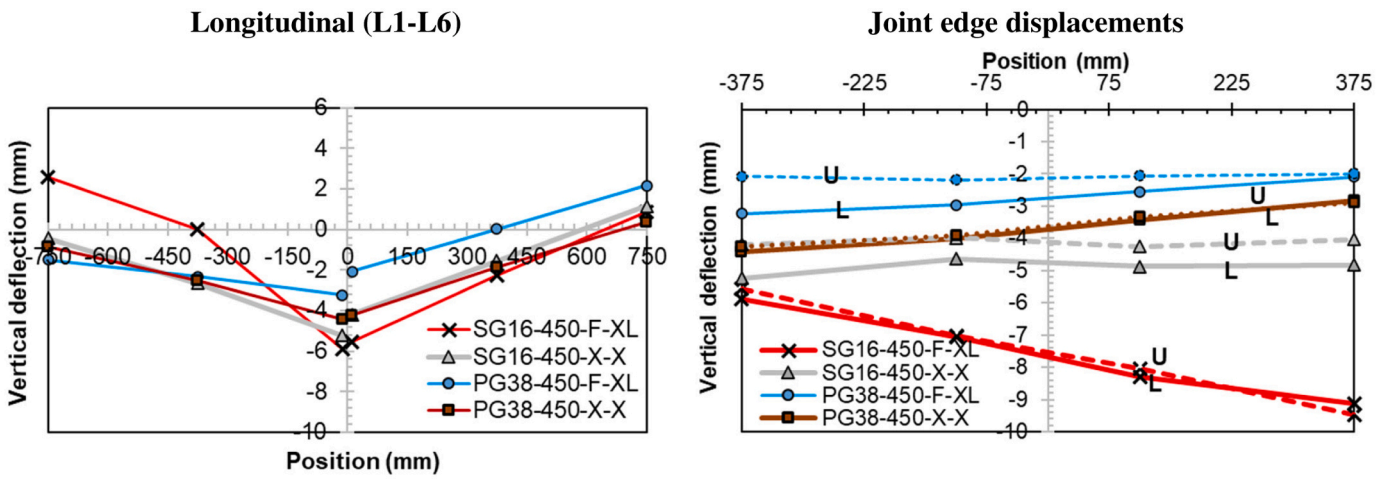

(g) vertical deflection profile at H10 (~35.6 kN) (GFRP dowels) (L: loaded slab; and U: unloaded slab)

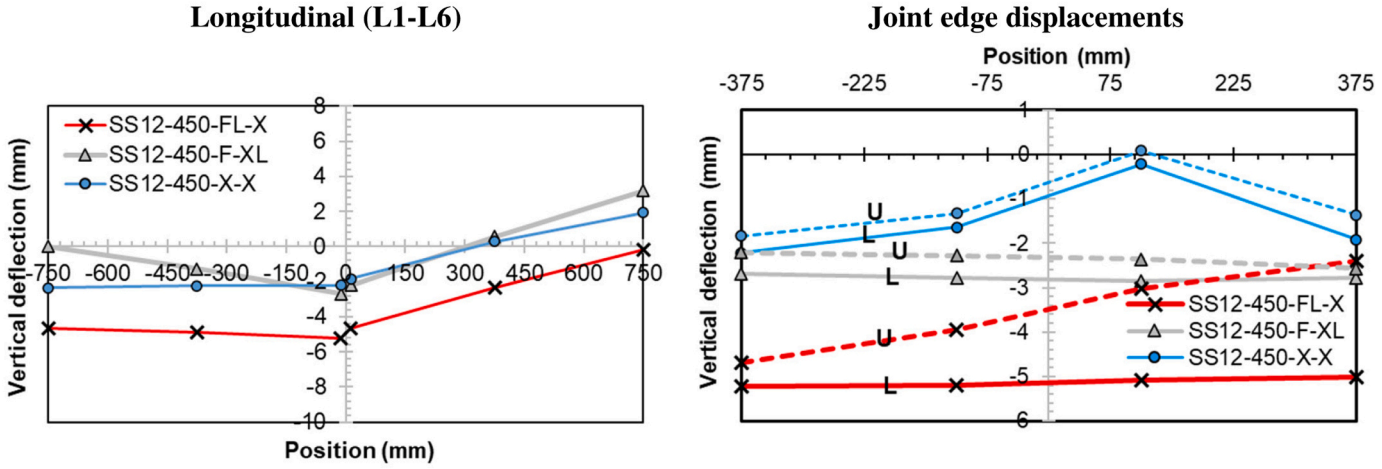

(h) vertical deflection profile at H10 (~35.6 kN) (SS12 dowels) (L: loaded slab; and U: unloaded slab)

Fig. 16. (*continued*).

Table 8
Effect of dowel end-fixity on E, LTE, and relative deflection at 35.6 kN load.

Specimen ID	Loaded slab, δ_l (mm)	Unloaded slab, δ_u (mm)	Joint effectiveness, *E* (%)	Load transfer efficiency, *LTE* (%)	Relative deflection, Δ (mm)
SG16-450-F-XL	5.86	5.52	97	94.2	0.34
SG16-450-X-X	3.99	3.34	91.1	83.7	0.65
PG38-450-F-XL	2.97	2.19	84.9	73.7	0.78
PG38-450-X-X	7.83	7.65	98.8	97.7	0.18
SS12-450-FL-X	5.06	3.85	86.4	76.1	1.21
SS12-450-F-XL	2.80	2.29	90	81.8	0.51
SS12-450-X-X	1.68	1.36	89.4	80.9	0.32

- GFRP dowel bars with diameters above 16 mm were found to be a feasible replacement to the more expensive stainless steel dowels, for light design wheel loads such as H10 (~35.6 kN).
- All dowel-jointed slabs tested in the study exhibited initial failures ranging between 50.8 kN and 100.8 kN, which are significantly higher than the H10 design wheel load of 35.6 kN.
- Three major modes of failure were observed: a) dowel bar shear failure with no bearing failure in concrete in smaller diameter dowels (PG14 and SG16); b) bearing failure in concrete without damage in the larger diameter GFRP dowel (PG38); and c) combined bearing and shear yielding in stainless steel dowel (SS12). The mode of failure in the specimens with smaller diameter dowels indicates that the design of dowels is not governed by bearing, which raises the need for a modified design equation for small-diameter GFRP dowels at joints in slabs-on-ground.
- Upon varying the dowel diameter from 14 mm to 38 mm, only an increase of 6.8% and 13.4% were observed in initial and ultimate failure loads. At 35.6 kN, the relative deflection in PG14 was 2.2 times that of PG38. Although the *E* and *LTE* of PG14 were comparable with PG38 up to 50 kN, at higher loads, the load transfer characteristics reduced significantly in PG14.
- When the spacing of the dowel was decreased from 250 mm to 200 mm, the initial and ultimate failure loads increased by 5.2% and 8.1%, respectively. The smaller spacing caused the relative

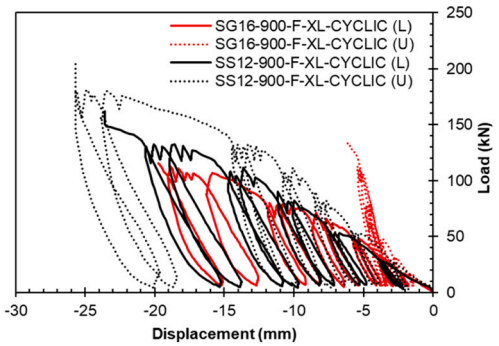

(a) SG16-900-F-XL-CYCLIC versus SS-900-F-XL-CYCLIC

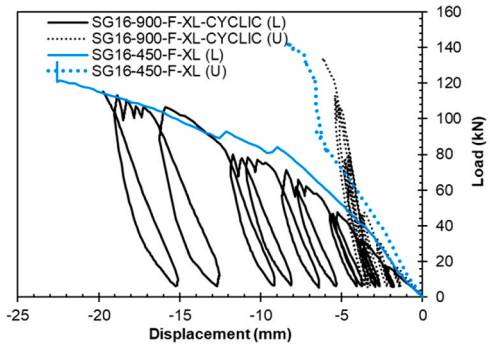

(b) SG16-900-F-XL-CYCLIC (cyclic) versus SG16-450-F-XL (static)

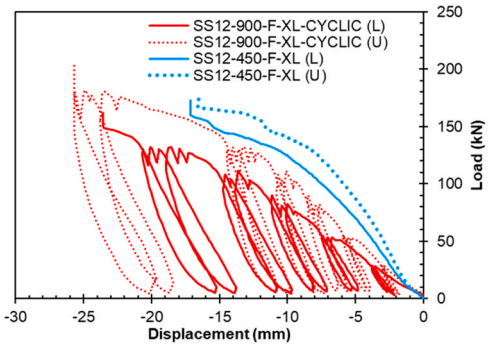

(c) SS12-900-F-XL-CYCLIC (cyclic) versus SS12-450-F-XL (static)

Fig. 17. Load-displacement plots of cyclic-loaded specimens.

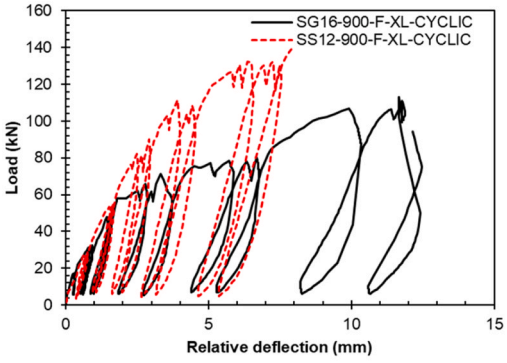

(a) Relative deflection

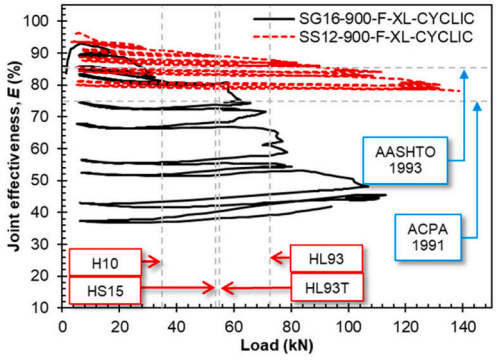

(b) Joint load effectiveness (*E*)

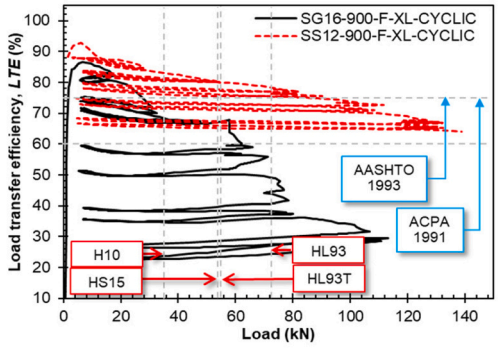

(c) Load transfer efficiency (*LTE*)

Fig. 18. Load transfer characteristics in SG16–900-F-XL and SS-900-F-XL specimens.

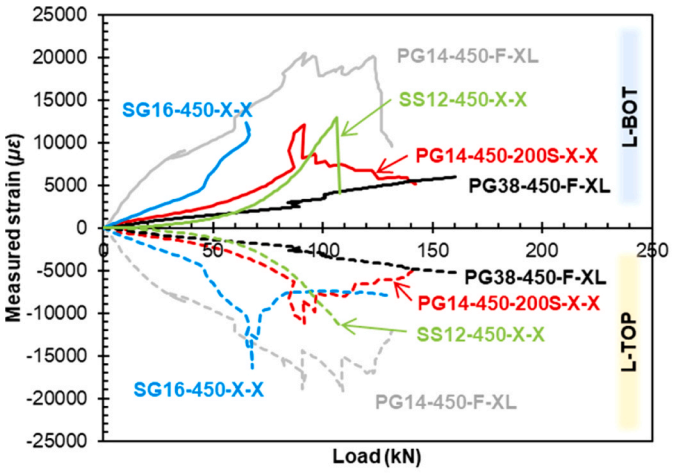

(a) Monotonic load tests: representative rebar strains in PG14, SG16, PG38, and SS12

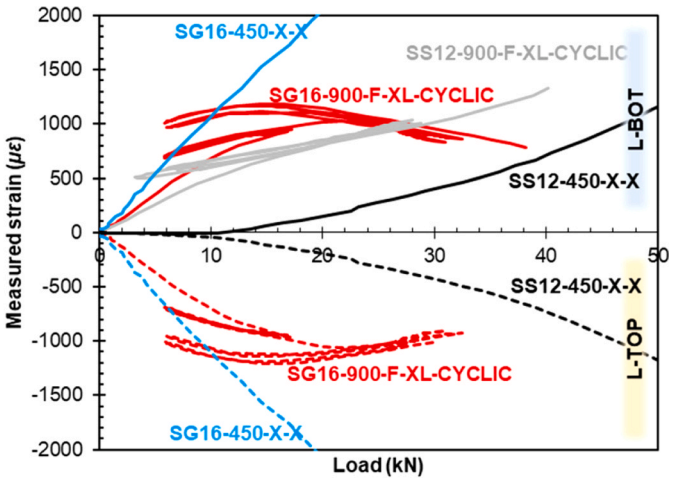

(b) Cyclic load tests dowel strains compared with monotonic

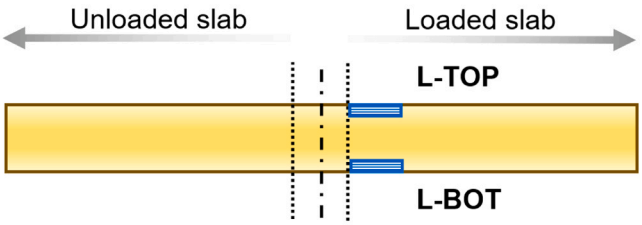

(c) position of L-TOP and L-BOT

Fig. 19. Dowel bar strains.

deflection (Δ) to decrease by 4.1 times, at a load of 35.6 kN. Also, the *E* and *LTE* values were found to increase by 8.5% and 16.2%, at a load of 35.6 kN.

- Increasing the length from 450 mm to 900 mm, caused initial and ultimate failures to decrease by 7.2% and 3.6%, respectively, while the relative deflection (Δ) at 35.6 kN was found to have reduced by 57.4%. However, the *E* and *LTE* values of 900 mm-length specimens were lower than the 450 mm-length specimens, but still within the ACPA limits.
- The dowel end-fixity F-XL showed a slightly higher stiffness, as compared to X-X and FL-X, in the load-displacement curves.
- Under cyclic loads, SG16 and SS12 exhibited initial failure loads of 55.5 kN and 50.8 kN, respectively, and ultimate loads of 133.2 kN and 179.0 kN, respectively. Up to 60 kN, the SG16 and SS12 showed similar behavior, and load transfer efficiencies were within AASHTO and ACPA limits.

CRediT authorship contribution statement

Fasil Mohammed: Writing – original draft, Visualization, Validation, Software, Investigation, Formal analysis, Conceptualization. **Rahman Muhammad K.:** Writing – original draft, Visualization, Validation, Software, Methodology, Investigation, Formal analysis, Conceptualization. **Al-Zahrani Mesfer M.:** Writing – review & editing, Supervision, Project administration, Methodology, Investigation, Funding acquisition. **Nanni Antonio:** Writing – review & editing, Visualization, Conceptualization. **Najamuddin Syed Khaja:** Investigation.

Declaration of Competing Interest

The authors declare that they have no known competing financial interests or personal relationships that could have appeared to influence the work reported in this paper.

Data availability

Data will be made available on request.

Acknowledgments

The authors would like to thank the Interdisciplinary Research Center for Construction and Building Materials (IRC-CBM), the Applied Research Center for Metrology, Standards and Testing (ARC-MST), and the Civil and Environmental Engineering Department at the King Fahd University of Petroleum and Minerals (KFUPM), Saudi Arabia for providing all the necessary support for conducting the research. The authors gratefully acknowledge the support provided by Saudi Aramco under contract No. 6600011900 for this research.

References

[1] Al-Humeidawi BH, Mandal P. Experimental investigation on the combined effect of dowel misalignment and cyclic wheel loading on dowel bar performance in JPCP. Eng Struct 2018;174:256–66. https://doi.org/10.1016/j.engstruct.2018.07.052.
[2] Asbahan RE, Vandenbossche JM. Effects of temperature and moisture gradients on slab deformation for jointed plain concrete pavements. J Transp Eng 2011;137:563–70. https://doi.org/10.1061/(ASCE)TE.1943-5436.0000237.
[3] Suo L., Wang B., Zheng C., Ma B. Dowels and Load Transfer Across Transverse Joints of Concrete Surface in Rigid Pavement 2013:1856–1861. ⟨https://doi.org/10.1061/9780784413159.268⟩.
[4] Harvey John, Ali Abdikarim Hassan, Hung David, Uhlmeyer Jeff, Popescu Lorina, Bush David, et al. Construction and test results from dowel bar retrofit HVS test sections 553FD, 554FD, and 555FD: US 101, Ukiah, Mendocino County. California: California Department of Transportation; 2003.

[5] William GW, Shoukry SN. 3D finite element analysis of temperature-induced stresses in dowel jointed concrete pavements. Int J Geomech 2001;1:291–307. https://doi.org/10.1061/(ASCE)1532-3641(2001)1:3(291).

[6] Benmokrane Brahim, Ahmed Ehab A, Montaigu Mathieu, Thebeau Denis. Performance of glass fiber-reinforced polymer-doweled jointed plain concrete pavement under static and cyclic loadings. Acids Struct J 2014;111:331–42.

[7] K.W. Anderson J.S. Uhlmeyer M. Russell C. Kinne J. Weston M. Davari et al. Glass Fiber Reinforced Polymer Dowel Bar Evaluation; 2012.

[8] Murison S, Shalaby A, Mufti A. Concrete-filled, glass fiber–reinforced polymer dowels for load transfer in jointed rigid pavements. Transp Res Rec 2005;1919: 54–64. https://doi.org/10.1177/0361198105191900107.

[9] Nanni A, De Luca A, Jawaheri Zadeh H. Reinforced concrete with FRP Bars. 0 ed.,. CRC Press; 2014. https://doi.org/10.1201/b16669.

[10] Zeng J-J, Liao J, Zhuge Y, Guo Y-C, Zhou J-K, Huang Z-H, et al. Bond behavior between GFRP bars and seawater sea-sand fiber-reinforced ultra-high strength concrete. Eng Struct 2022;254:113787. https://doi.org/10.1016/j.engstruct.2021.113787.

[11] Al-Humeidawi BH, Mandal P. Numerical evaluation of the combined effect of dowel misalignment and wheel load on dowel bars performance in JPCP. Eng Struct 2022;252:113655. https://doi.org/10.1016/j.engstruct.2021.113655.

[12] Al-Humeidawi BH, Mandal P. Evaluation of performance and design of GFRP dowels in jointed plain concrete pavement – part 1: experimental investigation. Int J Pavement Eng 2014;15:449–59. https://doi.org/10.1080/10298436.2013.824081.

[13] Löfsjögård M. A laboratory investigation on bonding properties of dowels in concrete roads. Mater Struct 2005;38:721–8. https://doi.org/10.1007/BF02484317.

[14] Max L. Porter Robert J. Guinn Jr. Andrew L. Lundy Dustin D. Davis John G. Rohner Investigation of Glass Fiber Composite Dowel Bars For Highway Pavement Slabs. Iowa: Highway Division of the Iowa Department of Transportation and Iowa Highway Research Board; 2001.

[15] Ahmed Shalaby, Scott Murison. Using Fiber-Reinforced Polymer Load Transfer Devices in Jointed Concrete Pavements, Orlando, Florida, USA; 2001.

[16] Bartholomew VLB, CL. FRP dowel bars in reinforced concrete pavements. Spec Publ 1993;138:813–30. https://doi.org/10.14359/10040.

[17] Design and Construction of Joints for Concrete Highways. ACPA. Skokie, Illinois: American Concrete Pavement Association (ACPA),; 1991.

[18] Guide for Design of Pavement Structures. Washington, D.C.: American Association of State Highway and Transportation Officials (AASHTO); 1993.

[19] ACI Committee 325. Structural design considerations for pavement joints July;53: 1–29.

[20] Friberg BF. Design of dowels in transverse joints of concrete pavements. Trans Am Soc Civ Eng 1940;105:1076–95. https://doi.org/10.1061/TACEAT.0005221.

[21] Timoshenko S, Lessells JM. Applied elasticity. 1st ed.,. East Pittsburgh, Pa: Westinghouse technical night school Press; 1925.

[22] P.V. Vijay H.V.S. GangaRao H. Li Design and Evaluation of Jointed Plain Concrete Pavement with Fiber Reinforced Polymer Dowels. McLean, VA: U.S. Department of Transportation Federal Highway Administration; 2009.

[23] Davis D, Porter M. Evaluation of glass fiber reinforced polymer dowels as load transfer devices in highway pavement slabs. Ames, IA: Proc. Transp. Conf.,; 1998. p. 78–81.

[24] Eddie D, Shalaby A, Rizkalla S. Glass fiber-reinforced polymer dowels for concrete pavements. Struct J 2001;98:201–6. https://doi.org/10.14359/10188.

[25] Li Hui. Evaluation of jointed plain concrete pavement (JPCP) with FRP dowels (M. S. Thesis). West Virginia University; 2004.

[26] Montaigu M. Caracterisation de goujons de polymeres renforces de fibres de verre (PRFV) pour les dalles de chaussee jointees. Universite de Sherbrooke; 2012.

[27] Øverli J. Experimental and numerical investigation of slabs on ground subjected to concentrated loads. Open Eng 2014;4. https://doi.org/10.2478/s13531-013-0159-9.

[28] Manfredi RP, Silva F de A, Cardoso DCT. On punching shear strength of steel fiber-reinforced concrete slabs-on-ground. Acids Struct J 2022;119:185–96. https://doi.org/10.14359/51734520.

[29] Salan EAV, Rahman MK, Al-Ghamdi S, Sakr J, Al-Zahrani MM, Nanni A. A monumental flood mitigation channel in Saudi Arabia. Concr Int 2021;43:33–41.

[30] Gardiner G. Composite reinforcing bars for future infrastructure. Concr Int 2021; 43:23–6.

[31] Cadenazzi T, Keles B, Rahman MK, Nanni A. Life-cycle cost and life-cycle assessment of a monumental fiber-reinforced polymer reinforced concrete structure. J Constr Eng Manag 2022;148:05022007. https://doi.org/10.1061/(ASCE)CO.1943-7862.0002339.

[32] C09 Committee. ASTM C39/C39M-21: test method for compressive strength of cylindrical concrete specimens. ASTM International; 2021. https://doi.org/10.1520/C0039_C0039M-21.

[33] C09 Committee. ASTM C496-96: test method for splitting tensile strength of cylindrical concrete specimens. ASTM International; 1996. https://doi.org/10.1520/C0496-96.

[34] Committee 325. ACI 325.12R-02: guide for design of jointed concrete pavements for streets and local roads. Farmington Hills, MI: American Concrete Institute (ACI); 2002.

[35] Maitra SR, Reddy KS, Ramachandra LS. Load transfer characteristics of dowel bar system in jointed concrete pavement. J Transp Eng 2009;135:813–21. https://doi.org/10.1061/(ASCE)TE.1943-5436.0000065.

[36] American Association of State Highway and Transportation Officials. In: LRFD bridge design specifications. 9th ed.,. Washington, DC: American Association of State Highway and Transportation Officials; 2020.

[37] Jaiswal S, Chauhan VB. Ultimate bearing capacity of strip footing resting on rock mass using adaptive finite element method. J King Saud Univ Eng Sci 2021. https://doi.org/10.1016/j.jksues.2021.09.004.

[38] M. Khan J. Wang Impact of Severe Drought on the Compacted Expansive Clays (Subgrade) in Northern Louisiana; 2017. https://doi.org/10.13140/RG.2.2.34898.86721/1.

[39] Avci B, Gurbuz A. Modulus of subgrade reaction that varies with magnitude of displacement of cohesionless soil. Arab J Geosci 2018;11:351. https://doi.org/10.1007/s12517-018-3713-1.

[40] Shapiro HI, Shapiro JP, Shapiro LK. Cranes and derricks. 3. ed.,. New York, NY: McGraw-Hill,; 2000.

[41] Tabatabaei Aghda ST, Ghanbari A, Tavakoli Mehrjardi G. Evaluating the applicability of geocell-reinforced dredged sand using plate and wheel load testing. Transp Infrastruct Geotechnol 2019;6:21–38. https://doi.org/10.1007/s40515-018-00067-2.

[42] Smith I. Smith's elements of soil mechanics. 10th ed.,. Hoboken, NJ: Wiley-Blackwell; 2021.

[43] Park D-W. Prediction of pavement fatigue and rutting life using different tire types. KSCE J Civ Eng 2008;12:297–303. https://doi.org/10.1007/s12205-008-0297-4.

[44] De Beer M., Fisher C., Jooste F.J. Determination of pneumatic tyre/pavement interface contact stresses under moving loads and some effects on pavements with thin asphalt surfacing layers; 1997.

[45] García JM, Bonett RL, Schultz AE, Carrillo J, Ledezma C. Flexural behavior of ungrouted post-tensioned concrete masonry beams with unbonded bars. Constr Build Mater 2019;203:210–21. https://doi.org/10.1016/j.conbuildmat.2018.12.101.

[46] Carrillo J, Oyarzo-Vera C, Blandón C. Damage assessment of squat, thin and lightly-reinforced concrete walls by the Park & Ang damage index. J Build Eng 2019;26:100921. https://doi.org/10.1016/j.jobe.2019.100921.

[47] Galati N, Nanni A, Gustavo Tumialan J, Ziehl PH. In-situ evaluation of two concrete slab systems. I: load determination and loading procedure. J Perform Constr Facil 2008;22:207–16. https://doi.org/10.1061/(ASCE)0887-3828(2008)22:4(207).

[48] Casadei P, Parretti R, Nanni A, Heinze T. In situ load testing of parking garage reinforced concrete slabs: comparison between 24h and cyclic load testing. Pr Period Struct Des Constr 2005;10:40–8. https://doi.org/10.1061/(ASCE)1084-0680(2005)10:1(40).

[49] ACI Committee 437. ACI 437: strength evaluation of existing concrete buildings. American Concrete Institute (ACI); 2019.

[50] Xargay H, Ripani M, Folino P, Núñez N, Caggiano A. Acoustic emission and damage evolution in steel fiber-reinforced concrete beams under cyclic loading. Constr Build Mater 2021;274:121831. https://doi.org/10.1016/j.conbuildmat.2020.121831.

[51] Durga Rajesh KV, Ram Prasad AVS, Munaf Shaik A, Buddi T. SEM with EDAX analysis on plasma arc welded butt joints of AISI 304 and AISI 316 steels. Mater Today Proc 2021;44:1350–5. https://doi.org/10.1016/j.matpr.2020.11.393.